Assessing the effects of restoration and conservation on gaseous carbon fluxes and climate mitigation potential across six European coastal wetlands

Miguel Cabrera-Brufau*[a], Camille Minaudo[a], Katrin Attermeyer[b], Alba Camacho-Santamans[a], Rafael Carballeira[c], Benjamin Misteli[b], Jorge Montes-Pérez[a], Daniel Morant[c], Biel Obrador[a], Antonio Picazo[c], Carlos Rochera[c], Mihai Adamescu[d], Raquel Ambrosio[e], Giancarlo Bachi[f], Nina Bègue[e], Martynas Bučas[g], Lídia Cañas Ramírez[a], Marco Carloni[f], Lamara Cavalcante[h], Constantin Cazacu[d], Giovanni Checcucci[f], J. Pedro Coelho[h], Valentin Dinu[d], Valtere Evangelista[f], Ilenia Férez Martín[a], Jonas Gintauskas[g], Relu Giuca[d], Anis Guelmami[e], Mirco Guerrazzi[f], Samuel Hilaire[e], Marija Kataržytė[g], Ana I. Lillebø[h], Raquel Lizán[c], Bruna R.F. Oliveira[h], Vitor H. Oliveira[h], Marta Pedrón[c], Jolita Petkuvienė[g], Tudor Racoviceanu[d], Michael Ronse[e], Chiara Santinelli[f], Ana I. Sousa[h], Wouter Suykerbuyk[i], Edvinas Tiškus[g], Claudia Tropea[f], Diana Vaičiūtė[g], Silvia Valsecchi[f], Marinka van Puijenbroek[i], Mourine J. Yegon[b], Antonio Camacho[c†], Daniel von Schiller[a†]

[a] Departament de Biologia Evolutiva, Ecologia i Ciències Ambientals, Universitat de Barcelona, Av. Diagonal 643, 08028, Barcelona, Spain

[b] WasserCluster Lunz - Biologische Station, Dr. Carl Kupelwieser Promenade 5, 3293, Lunz am See, Austria

[c] Institut Cavanilles de Biodiversitat i Biologia Evolutiva, Universitat de València, C/Catedràtic José Beltran 2, 46980, Paterna, Spain

[d] Department of Systems Ecology and Sustainability, University of Bucharest, spl. Independentei 91 - 95, 50095, Bucharest, Romania

[e] Institut de recherche pour la conservation des zones humides méditerranéennes, Tour du Valat, Le Sambuc, 13200, Arles, France

[f] Istituto di Biofisica, Consiglio Nazionale delle Ricerche (CNR) Pisa, Via Giuseppe Moruzzi 1, 56124, Pisa, Italy

[g] Marine Research Institute, Klaipėda University, Universiteto ave. 17, 92294, Klaipėda, Lithuania

[h] ECOMARE, CESAM - Centre for Environmental and Marine Studies, Department of Biology, University of Aveiro, Campus de Santiago, 3810-193, Aveiro, Portugal

[i] Wageningen Marine Research, Wageningen University & Research, Korringaweg 7, 4401 NT, Yerseke, The Netherlands

[†]These authors share last authorship as research heads

*Corresponding author, email: miguelcabrera@ub.edu

Version notice: This document is the author's accepted manuscript (AAM), corresponding to the peer-reviewed version accepted for publication in *Ecological Engineering* on **29 June 2026**. It is a non-typeset version and may differ from the final published article in formatting and copy-editing. Please cite the published version of record once available.

Abstract

Coastal wetlands play a substantial role in regulating Earth's climate through exchanges of greenhouse gases (GHGs). Current European policies promote widespread coastal wetland restoration to reverse historical losses and ongoing pressures. However, substantial uncertainty remains regarding how carbon dioxide (CO_2) and methane (CH_4) fluxes respond to restoration across different coastal wetland types and whether these responses translate into net climate mitigation in terms of CO_2 equivalents (CO_2-eq). We measured simultaneous CO_2 and CH_4 fluxes using static chambers across four seasons at multiple locations spanning preserved, altered and restored sites within six European coastal wetlands of different ecological types. By comparing GHG exchanges and resulting CO_2-eq balances across wetlands, we identified dominant biogeochemical drivers of CO_2 and CH_4 dynamics and assessed the climate mitigation potential of conservation and restoration actions. CO_2 fluxes were primarily controlled by landscape-scale vegetation cover and inundation, whereas CH_4 emissions responded to less evident changes in water quality, salinity and wetland hydrodynamics. Comparisons of CO_2-eq balances between altered and restored sites showed that seagrass replantation was associated with significant mitigation potential under both 100-year and 20-year CH_4 warming scenarios, while eutrophication reversal through improved water treatment was only significant under the 20-year scenario. In contrast, other restoration measures modified CO_2 and CH_4 fluxes in opposing directions, resulting in no significant net change in combined CO_2-eq balances. Overall, our results demonstrate that climatic responses to coastal wetland restoration are both GHG-specific and wetland-type dependent, underscoring the need for tailored restoration strategies and robust, multi-GHG monitoring to detect and accurately quantify potential climatic benefits.

Keywords: coastal wetlands, ecological restoration, CO_2 fluxes, CH_4 fluxes, climate change mitigation

1. Introduction

Coastal wetlands are relevant components of the global carbon (C) cycle and are widely recognized as blue carbon ecosystems. Despite their relatively low areal extent, they exert a disproportionate influence on the global climate by providing long-term C-sequestration and regulating atmospheric greenhouse gas (GHG) concentrations (Mitsch et al., 2013). Wetlands in good conservation status are highly productive ecosystems, where low oxygen availability limits aerobic organic matter degradation, resulting in net uptake of carbon dioxide (CO_2) and sequestration of C in sediments and biomass (Reddy et al., 2022). At the same time, wetland anoxic sediments act as hot spots for methane (CH_4) emissions, making up 20-30% of global CH_4 emissions (Saunois et al., 2016), particularly when they are degraded by alterations enriching the organic content such as eutrophication (Morant et al., 2020a, 2020b). While the magnitude of CO_2 exchanges typically exceeds that of CH_4, the higher global warming potential of the latter has the potential to overcome the effects of CO_2 uptake and might result in a net balance that favours atmospheric warming (Canadell and Monteiro, 2023). Ultimately, the net radiative forcing of coastal wetlands is largely determined by the net balance of CO_2 and CH_4 exchanges with the atmosphere.

Diverse historical and current pressures have led to important reductions of the extent and quality of global wetland ecosystems (Fluet-Chouinard et al., 2023). While areal loss quantification remains challenging, especially when assessing coastal zones with high historical development and land-reclamation practices, estimates of European coastal wetland loss exceed 65% during the last century (Airoldi and Beck, 2007). Further, the majority of remaining European standing water bodies have a poor or bad ecological status (European Environment Agency, 2024) and experience diverse natural and anthropogenic pressures (Maes et al., 2020). Although conservation policies, such as those under Ramsar (Ramsar Convention, 1971) and the EU habitats Directive, help preserve the remaining wetlands, their historical losses mean that widespread restoration is still needed. In this context, the recent EU Nature Restoration Regulation aims at reverting this widespread degradation and recovering crucial ecosystems services lost (European Union, 2024). Among the potential benefits of restoration, climate change mitigation is increasingly being used as a supporting argument. However, large uncertainties remain on the climatic mitigation capacity of coastal wetland restoration (Jones et al., 2024).

Coastal wetlands influence climate primarily through CO_2 and CH_4 exchange, governed by the balance among photosynthesis, aerobic and anaerobic respirations releasing CO_2, as well as methanogenesis (Reddy et al., 2022). While local climate and wetland type shape baseline GHG fluxes (Camacho et al., 2017), ecosystem alteration and restoration can modify these fluxes by changing key controls, including vegetation, nutrient inputs, hydrology, salinity, and sediment redox conditions (Camacho-Santamans et al., 2025; Morant et al., 2024). The biomass and type of dominant primary producers exert a large impact on the primary productivity of wetlands, as they represent the basic functional standing stock for photosynthetic CO_2 uptake. While nutrients are essential to maintain plant photosynthetic rates, excessive nutrient loads, namely nitrogen and phosphorus, can lead to eutrophication and uncontrolled proliferation of benthic algae and phytoplankton blooms (Zilius et al., 2014). This shift in primary producers results in a cascade of biogeochemical consequences, including anoxia and organic matter degradation through methanogenesis, that ultimately lead to severely enhanced CH_4 emissions (Bonaglia et al., 2025). Wetland hydrology is one of the key factors regulating ecosystem functioning, as it influences both primary production through water availability and the balance between

respiration and methanogenic degradation of organic matter through limitation of oxygen diffusion into the sediments (Cui et al., 2024; Rochera et al., 2025). However, anoxic conditions do not always result in elevated wetland CH_4 emissions, as the supply of sulphate by saline waters can severely limit methanogenesis through resource competition with more energy-efficient sulphate reduction metabolisms under the right redox conditions (Lovley and Klug, 1983; Miralles-Lorenzo et al., 2025). Emissions of CH_4 are further modulated by the existence of plant-mediated transport mechanisms, which can bypass oxidation back to CO_2 during upward diffusion through oxic sediment horizons (Ge et al., 2024).

While the general biogeochemical controls of wetland CO_2 and CH_4 exchanges are relatively well understood, large uncertainty remains on how these interact under practical cases of ecological restoration, leading to poorly constrained climatic mitigation potential (Griscom et al., 2017). Wetland restoration generally enhances CO_2 uptake outweighing increases in CH_4 emissions and resulting in net climate benefits (He et al., 2024). However, existing literature is dominated by studies focused on inland systems (peatlands) and on just a few coastal wetland types (mangroves, saltmarshes), which do not capture coastal wetland diversity accurately (Misteli et al., 2025; Taillardat et al., 2020). Other synthesis efforts on coastal wetland restoration focus exceedingly on C sequestration (i.e., Blue Carbon), overlooking the large role of CH_4 emissions on the net climatic outcome of wetland restoration (Bertolini and da Mosto, 2021). In addition, while valuable for identifying broad patterns, global syntheses often aggregate the high diversity of wetland types, alteration histories and restoration strategies into a limited number of categories (O'Connor et al., 2020), thereby obscuring relevant contextual factors and limiting process-based effective transferable knowledge for management. Overall, current evidence is still scarce on how coastal wetland restoration influences GHG fluxes (Macreadie et al., 2019; Misteli et al., 2025) and coordinated, multi-site assessments are needed to reveal common controls that are robust across wetland types and restoration pathways.

In order to better understand the climate mitigation potential of restoring and conserving European coastal wetlands, this study examines concomitant CO_2 and CH_4 exchanges and their combined carbon dioxide equivalent (CO_2-eq) climatic effect across six diverse European case pilot coastal wetlands: saltmarshes, seagrass meadows, freshwater and brackish marshes, riverine lakes and freshwater coastal lagoons. By explicitly embracing the diversity of coastal wetland types, conservation status, and restoration pathways represented across Europe, we aim to move beyond site-specific assessments and identify common patterns and drivers governing GHG flux responses to alteration and restoration. Using standardized static chamber measurements conducted during four seasonal sampling campaigns, we compare instantaneous GHG exchanges across wetland sites representative of preserved, altered, and restored status. Our objectives are to (i) systematically identify the main biogeochemical drivers controlling CO_2 and CH_4 fluxes in the main European coastal wetland types, and (ii) quantify the extent to which restoration and conservation modify their net climatic effect, expressed as daily CO_2-eq fluxes. We hypothesize that (i) the drivers and sensitivity of GHG fluxes to the conservation status differ between CO_2 and CH_4, reflecting their distinct production and consumption pathways, and that (ii) the net climatic response to restoration depends on both the type of anthropogenic alteration and the wetland type considered. At the same time, we expect that consistent cross-system patterns will emerge, allowing the identification of shared controls on GHG fluxes despite the heterogeneity of wetland types and restoration contexts examined.

2. Methods

2.1. Study areas

Six case pilots were strategically selected to cover a wide range of European coastal wetland types, thereby providing a representative sample of the ecosystem and climatic diversity across the continent, covering major European coastlines (Atlantic, Mediterranean, Black Sea, Baltic Sea). The selected case pilots were (**Figure 1, Figure S1**): South-West Dutch Delta (DU, intertidal salt marshes, Netherlands), Ria de Aveiro (RI, intertidal seagrass beds, Portugal), Camargue (CA, freshwater marshes and ponds, France), the Valencian wetland Marjal dels Moros (VA, brackish marshes, Spain), Danube Delta (DA, freshwater lakes and ponds with reed beds, Romania) and Curonian Lagoon (CU, freshwater lagoon with reed and submerged vegetation, Lithuania). Within each case pilot, sites representing three conservation statuses were selected in duplicate: preserved, altered, and restored. Preserved sites served as reference systems with unaltered structure and function, whereas altered and restored sites reflected wetland-specific dominant anthropogenic pressures and corresponding restoration measures. Accordingly, the "restored" category represents context-dependent interventions linked to the ecological functioning and alteration history of each wetland system rather than a standardized restoration approach across case pilots. Sites within each pilot wetland were geographically close, ensuring comparable climatic conditions and allowing differences in biogeochemical functioning to be attributed to the conservation status. Site characteristics are summarized in **Table 1**, with further details provided in **supplementary materials** and in Oliveira et al. (2026).

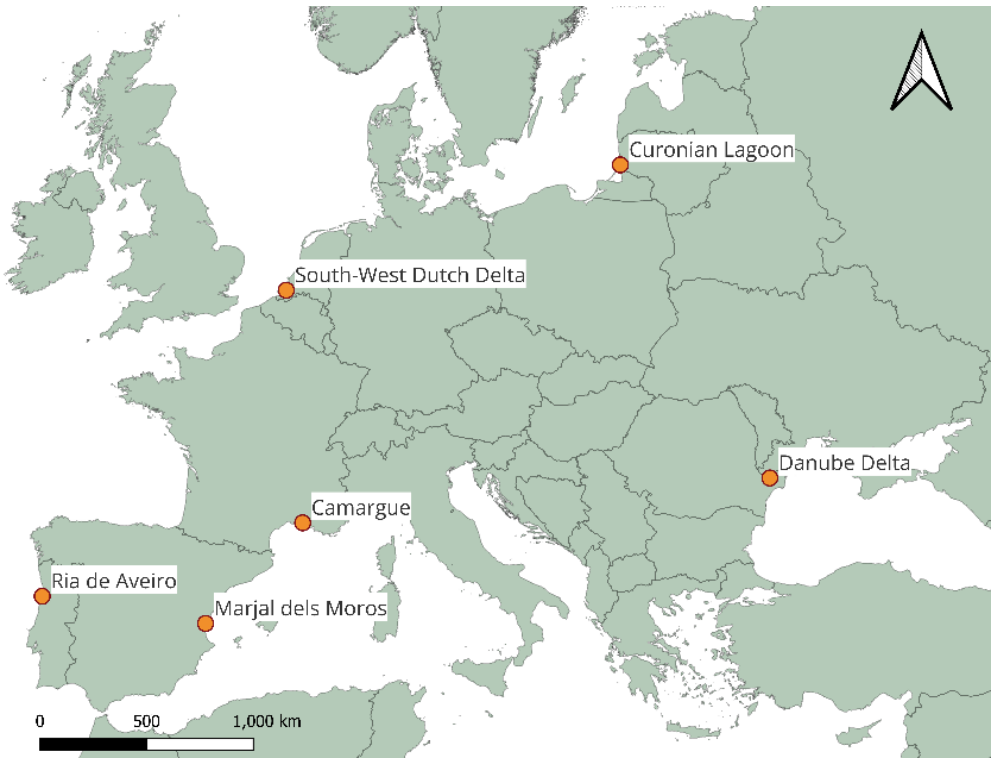

Figure 1. Map showing the location of the six case pilots. Map lines do not necessarily depict accepted national boundaries. Representative pictures can be found in **Figure S1**.

Table 1. Summary descriptions of studied wetland type, main alterations and restoration activities for each of the six case pilots.

Case pilot	Wetland type	Alteration	Restoration
South-West Dutch Delta (DU)	Intertidal salt marshes	Erosion-protection coastal infrastructures	Removal of barriers and passive saltmarsh recovery
Ria de Aveiro (RI)	Intertidal *Zostera noltii* seagrass meadows	Bait-digging, trampling, vegetation loss	Active re-vegetation (transplantation)
Camargue (CA)	Freshwater marshes and ponds	Land-use change and artificial hydrological regime	Habitat reconstruction (Soil, hydrology, morphology, vegetation)
Marjal dels Moros (VA)	Brackish marshes	Desalination, hydromorphological and soil degradation, invasive species	Habitat reconstruction (Soil, hydrology, morphology, vegetation)
Danube Delta (DA)	Freshwater lakes and ponds with reed beds	Land-use change (crops and livestock)	Habitat reconstruction (hydrology, morphology, vegetation)
Curonian Lagoon (CU)	Freshwater littoral with submerged vegetation and reed beds	Water quality (eutrophication)	Passive restoration through the reduction of nutrient load and hydrological changes.

2.2. Sampling design

A standardized sampling protocol using static chamber GHG flux measurements was applied across all case pilot wetlands (Minaudo et al., 2023). All 36 sites were sampled once per season, between October 2023 and August 2024. In each site, the areal proportion of three land cover strata classes was estimated in advance using aerial photography and remote sensing images, then confirmed visually upon arrival: (i) open water areas (i.e., without emergent vegetation and with >10 cm of water depth), (ii) vegetated areas (i.e., covered by emergent vegetation (helophytes, and, for Ria de Aveiro, seagrasses), regardless of water presence), and (iii) bare areas (i.e., covered by soil or sediment exposed to the atmosphere at the sampling time). Strata representing <10% of the site area at the time of the visit were excluded from sampling. Each remaining stratum was sampled with a minimum of 3 static chamber deployments, with additional deployments allocated proportionally to stratum areal cover and randomly distributed within each of them. On each sampling day, an average of 15 ± 2 (mean ± SD) chamber deployments per site were performed, depending on logistical constraints.

All chamber deployments included a dark incubation to minimize heating effects (Lorke et al., 2015). In vegetated areas, an additional transparent incubation was performed to assess the effects of photosynthesis on GHG fluxes. Concentrations of CO_2, CH_4, and H_2O were measured by recirculating chamber headspace through portable gas analyzers (Li-COR 7810, Picarro G4301, GLA132-GGA). Incubation start and end times were recorded manually and, whenever possible, via instrument software. Two different custom-built static chambers were used depending on the strata. Open water fluxes were measured using a floating opaque semi-spherical chamber (V = 14.4 L, A= 1134 cm2, **Figure S2**) with 10-15 min incubations to capture diffusive and ebullitive fluxes. Bare and vegetated areas were sampled using a modular transparent cylindrical plexiglass chamber with 3-5 min incubations; collars were inserted 1-3 cm into the sediment and dark conditions were ensured by covering the chamber with an opaque blanket. Chamber volume (V = 4.6 to 69 L, A= 460 cm2, **Figure S2**), was adjusted to vegetation height to optimize sensitivity. In flooded vegetated areas, and to avoid mobilization of sediment CH_4, the chamber was maintained on the water surface either using a flotation ring (**Figure S2**) or holding it by

hand. Effective chamber volume was calculated for each deployment based on chamber height above the water and sediment surface.

2.3. Flux calculation

2.3.1. Instantaneous flux estimates

All data treatment, including flux calculations and statistical analyses, was performed in R version 4.5.0 (R Core Team, 2025). Incubation time periods were mapped onto the raw gas concentration time series and start-end times adjusted to exclude instrument and manipulation artefacts after individual visual inspection of each incubation. Ebullitive patterns of CH_4 timeseries were identified but not excluded. A total of 52 CO_2 (1.7%) and 56 CH_4 (1.8%) time series were discarded due to severe artifacts or documented manipulation errors. For the remaining 2,990 CO_2 and 2,986 CH_4 time series, instantaneous fluxes were estimated independently for each gas species using three approaches: (i) a two-point method, where the flux was calculated from the net concentration change throughout the incubation using the average (10 s) initial and final concentrations; (ii) a linear model (LM); and (iii) a non-linear (HM) (Hutchinson and Mosier, 1981) regression model. LM and HM models were obtained using the goFlux R package v2.0.0 (Rheault et al., 2024). Areal molar fluxes were calculated for each of the three approaches via the ideal gas law using chamber geometry, and site-specific temperature and atmospheric pressure recorded by the nearest meteorological station. For each gas time series, a best-flux estimate was selected from the three available models following sequential objective criteria (see **supplementary materials**). The resulting dataset, containing 2,990 CO_2 and 2,986 CH_4 instantaneous fluxes from 2,106 static chamber deployments, is deposited at LifeWatch ERIC (Cabrera-Brufau et al., 2025). The unprocessed GHG concentration time-series dataset is deposited at Zenodo (Cabrera-Brufau et al., 2026) and code for reproduction of the instantaneous flux dataset is available through the GitHub repository (Cabrera-Brufau and Minaudo, 2026).

2.3.2. Data filtering and pooling of non-vegetated strata

To ensure comparability across case pilots and conservation statuses, deployments conducted outside site boundaries or after substantial manipulation (e.g., vegetation removal) were discarded (54 deployments). In the two tidally influenced case pilots (Ria de Aveiro and Dutch delta), deployments during rising and receding tides were also discarded (93 deployments), due to the transient nature of peak-fluxes under these conditions (Lin et al., 2024) and the difficulty of attributing them to the conservation status of the location where they were obtained. Therefore, all subsequent analyses for these case pilots refer only to low-tide conditions. Overall, 147 of the 2,106 deployments with valid fluxes (7%) were excluded from further analysis. Additionally, to ensure strata representativity across statuses and seasons within each case pilot, the three sampled strata were pooled into two classes based on the presence or absence of emergent vegetation (vegetated vs. non-vegetated), enabling robust assessment of strata-specific status effects.

2.3.3. Daily temporal integration and calculation of CO_2 equivalent flux

Instantaneous fluxes were temporarily integrated into a single net daily flux for each chamber deployment, accounting for stratum-specific incubation availability. For vegetated strata, net daily fluxes were calculated by scaling transparent and dark instantaneous fluxes to the respective daytime and nighttime fractions at each site and date, based on official sunrise and sunset times calculated with the suncalc R package (Thieurmel and Elmarhraoui, 2022). For non-vegetated strata, net daily fluxes were derived either directly from a single dark instantaneous

measurement (1,087 chambers, 94.7%) or, when both dark and transparent incubations were available due to visible microphytobenthos (61 chambers, 5.3%), using the same temporal scaling approach applied to vegetated strata. Daily combined climatic effects as CO_2 equivalent (CO_2-eq) flux were calculated for each chamber deployment using the daily CO_2 and CH_4 fluxes and applying the global warming potential (GWP) factors for CH_4 mass flux of either 27 or 79.7 for 100-year or 20-year time horizons, respectively (IPCC, 2023). In total, 1,917 CO_2, 1,916 CH_4, and 1,887 CO_2-eq daily fluxes were obtained. Fluxes are reported as daily molar CO_2 and CH_4 fluxes per unit area and time, or as daily CO_2-eq mass fluxes per unit area and time (Neubauer, 2021).

2.4. Statistical treatment

To assess the effects of the conservation status on GHG fluxes, generalized linear mixed effects models (GLMM) were independently built for daily CO_2 and CH_4 fluxes for each case pilot. Flux data was transformed using the bestNormalize package (Peterson, 2021), selecting the transformation that maximized normality for each dataset. In addition to the default transformation options, a pseudo-log transformation from the scales package (Wickham et al., 2025) was included, allowing continuous treatment of positive and negative fluxes while transitioning to linear scaling near zero. Daily flux was modelled as a function of conservation status, season, vegetation presence, and their interactions as fixed effects, while site was included as a random intercept to account for repeated seasonal sampling and site-specific variability. Gaussian-distribution models were preferentially used; t-family models were used when gaussian model assumptions were not met. For Ria de Aveiro, vegetation presence was excluded from the fixed-effects structure due to the absence of non-vegetated areas in restored sites. Models were fitted using the glmmTMB package (McGillycuddy et al., 2025) and validated using DHARMa diagnostics (Hartig, 2024).

Estimated marginal means (EMMs) were obtained using the emmeans package (Lenth, 2025). For models including vegetation presence, EMMs were weighted according to the seasonal proportional cover of vegetated and non-vegetated areas, while maintaining equal weighting across seasons for annual estimates. For Ria de Aveiro, equal seasonal weights were applied. A paired parametric bootstrap approach was implemented independently for each case pilot to improve the robustness of model-derived estimates. The paired structure additionally allowed uncertainty from CO_2 and CH_4 models to be propagated into combined climate metrics (CO_2-eq). Using the fitted CO_2 and CH_4 models, 5000 paired bootstrap iterations were generated by simulating new response values while preserving the original sampling design, predictor structure, and correspondence between gases. For each bootstrap iteration, EMMs were recalculated for both gases, yielding paired model-scale distributions for all relevant predictor combinations (i.e., status, status within season and status within vegetated and non-vegetated conditions).

To quantify the magnitude of CO_2 and CH_4 fluxes at each predictor level, bootstrap EMM distributions for each gas were back-transformed to the original molar flux scale, from which mean estimates, standard errors (SE), and 95% confidence intervals (CI95) were calculated. To quantify flux differences between predictor levels, pairwise contrasts were calculated from these back-transformed distributions and mean, SE, and CI95 values were calculated. The significance of these comparisons was assessed on model scale by recalculating the pairwise contrasts from the bootstrap EMM distributions. Empirical two-sided p-values were derived directly from bootstrap contrast distributions. P-values were adjusted for multiple comparisons using the Holm correction method.

To estimate combined climate forcing, paired bootstrap distributions of back-transformed CO_2 and CH_4 fluxes were converted into CO_2-eq fluxes using both 100-year and 20-year global warming potential scaling factors for CH_4. For each bootstrap iteration, paired CO_2 and scaled CH_4 estimates were summed, preserving the correspondence between gases across simulations and generating paired distributions of CO_2-eq exchanges. From these paired real-scale CO_2-eq distributions, EMMs and pairwise contrasts were calculated, together with their associated SE and CI95. Empirical p-values for CO_2-eq contrasts were derived directly from the bootstrap contrast distributions and adjusted with Holm correction. Thus, while significance testing for CO_2 and CH_4 contrasts was performed on their respective model scales, the significance of combined CO_2-eq contrasts was assessed on the real scale.

All figures were produced with ggplot2 package (Wickham, 2016). A significance threshold of $\alpha = 0.05$ was applied for all statistical tests. Different letters (Compact Letter Display, CLD) were assigned to significantly different EMMs groups in figures using the multcompView package (Graves et al., 2024). The scripts used for statistical analyses and figure generation are archived at Zenodo (https://doi.org/10.5281/zenodo.21129514).

2.5. Methodological considerations

Several limitations affect the representativeness of the GHG flux estimates presented. Static chamber measurements are prone to closing/opening artefacts and non-linear patterns (Maier et al., 2022). These were mitigated through careful handling, timeseries screening, and standardized flux selection, ensuring transparent processing and minimizing subjective biases (Minaudo et al., 2026). While our approach allowed estimation of CH_4 fluxes in the presence of ebullitive dynamics, it is important to recognize that ebullition is a stochastic emission pathway over the short temporal scales of chamber deployments and is generally better constrained by methods integrating fluxes over longer periods, such as bubble traps (Wik et al., 2013). Nevertheless, this source of variability was partially mitigated through the high replication of chamber measurements, which is often logistically challenging for bubble-trap approaches. Spatially, the highly localized nature of chamber measurements may result in substantial variability of wetland-level average fluxes. This was accounted for by the stratified sampling design, ensuring good representation of relevant strata while allowing for the detection of strata-specific effects. Nevertheless, while the employment of modular chambers allowed for coverage of most strata, their dimensions precluded the sampling of large (>1.5 m) vegetation stands, likely resulting in underestimations of CO_2 uptake for reed dominated sites. Temporally, sampling was limited to one low-tide event per season and relied on opaque chambers instead of direct night-time measurements. Consequently, the seasonal patterns reported here should not be interpreted as robust representations of true climatic seasonality, as they reflect both seasonal and short-term meteorological variability. Similarly, the integration of daily fluxes from paired dark and transparent chamber measurements does not fully capture diel variability in GHG exchange and may introduce biases associated with differences between dark chamber conditions and true night-time ecosystem functioning. Finally, our measurements were restricted to surface-atmosphere GHG exchanges and therefore do not account for potential lateral GHG transport through surface-water or groundwater pathways (Sadat-Noori et al., 2025), which may represent important additional components of whole-system GHG budgets (Schutte et al., 2020). Accordingly, the approach was not intended to generate fully scalable site-level GHG budgets, but to enable consistent comparisons across conservation statuses to assess how wetland-specific alteration and restoration pathways influence GHG exchanges and potential climate mitigation signals.

3. Results

3.1. Fluxes across preserved wetlands

Daily net fluxes at preserved sites varied among case pilot wetlands and GHG species (**Figure 2**). Preserved sites generally exhibited daily CO_2 fluxes (mmol CO_2 m^{-2} d^{-1}) centred around zero but with substantial variability (**Figure 2a**). Atlantic tidal sites DU (median = -23.6, IQR = -214 to 17.1) and RI (median = -32.6, IQR = - 56 to -18.2), showed net CO_2 uptake, with DU presenting one of the largest flux variabilities. Mediterranean sites exhibited similarly high variability, with CA showing the highest CO_2 flux (median = 15.7, IQR = -57.2 to 86) and VA having CO_2 fluxes closest to net zero (median = 2.0, IQR = -30.3 to 67.2). Eastern sites showed similar CO_2 flux profiles, with intermediate median fluxes and relatively low variability for DA (median = 6.1, IQR = -4.9 to 24.4) and slightly higher fluxes for CU (median = 9.2, IQR = -0.8 to 36.4).

Net daily CH_4 fluxes (mmol CH_4 m^{-2} d^{-1}) were generally positive across all preserved sites, with higher median emissions associated with greater variability and strongly skewed distributions (**Figure 2b**). Atlantic tidal wetlands showed the lowest CH_4 emissions, with similar values at DU (median = 1.5 x 10^{-3}, IQR = -4.2 x 10^{-3} to 1.6 x 10^{-2}) and RI (median = 8.0 x 10^{-3}, IQR = 4.3 x 10^{-3} to 1.2 x 10^{-2}). Mediterranean preserved sites exhibited intermediate CH_4 emissions, with CA (median = 1.7 x 10^{-2}, IQR = 1.9 x 10^{-3} to 1.5 x 10^{-1}) showing lower median fluxes than VA (median = 3.4 x10^{-2}, IQR = 3.4 x10^{-3} to 1.3 x 10^{-1}) but comparable variability. Eastern preserved sites showed the highest emissions, with DA (median = 1.1, IQR = 0.7 to 9.9) displaying the highest CH_4 fluxes and extreme skewness, while CU (median = 0.8, IQR = 0.4 to 1.7) had lower and less variable CH_4 fluxes.

The contrasting CO_2 and CH_4 flux profiles at preserved sites resulted in CO_2-eq distributions reflecting the dominant contributor to climatic forcing in each case pilot under both 100-year and 20-year GWP scaling factors for CH_4 (**Figure 2c)**. CO_2 generally dominated the 100-year CO_2-eq balance, with CH_4 contributing minor proportions (mean ± SD) in Atlantic (2 ± 5% in both DU and RI) and Mediterranean wetlands (7 ± 19% in CA, 7 ± 17% in VA), but substantially larger shares in eastern wetlands (49 ± 32% in DA, 34 ± 27% in CU). Regarding 100-year GWP CO_2-eq fluxes (g CO_2 eq. m^{-2} d^{-1}), values were lowest in the Atlantic tidal wetlands RI (median = -1.5, IQR = -2.5 to -0.9) and DU (median = -1.0, IQR = -9.1 to 0.8), intermediate in the Mediterranean wetlands CA (median = 0.8, IQR = -1.2 to 4.2) and VA (median = 0.3, IQR = -1.0 to 3.1), and highest in the eastern wetlands DA (median = 1.0, IQR = 0.2 to 3.8) and CU (median = 0.9, IQR = 0.3 to 2.3). The relative contributions of CH_4 to the CO_2-eq balances increased markedly under the 20-year GWP scenario, particularly in freshwater eastern wetlands, reaching 65 ± 30% in DA and 52 ± 28% in CU. Mediterranean wetlands showed intermediate CH_4 contributions (12 ± 23% for both CA and VA), whereas Atlantic wetlands remained comparatively low despite increased variability (3 ± 10% for DU and 3 ± 9% for RI). Under the 20-year GWP scenario, tidal wetlands showed only minor changes in CO_2-eq fluxes (RI: median = -1.5, IQR = -2.5 to -0.9; DU: median = -0.9, IQR = -9.1 to 0.8). Mediterranean systems showed moderate increases (CA: median = 1.1, IQR = -0.4 to 4.7; VA: median = 0.4, IQR = -0.9 to 3.2), while the largest increases under the 20-year GWP scenario occurred in eastern wetlands, including DA (median = 1.9, IQR = 0.8 to 6.0) and CU (median = 1.6, IQR = 0.6 to 4.1).

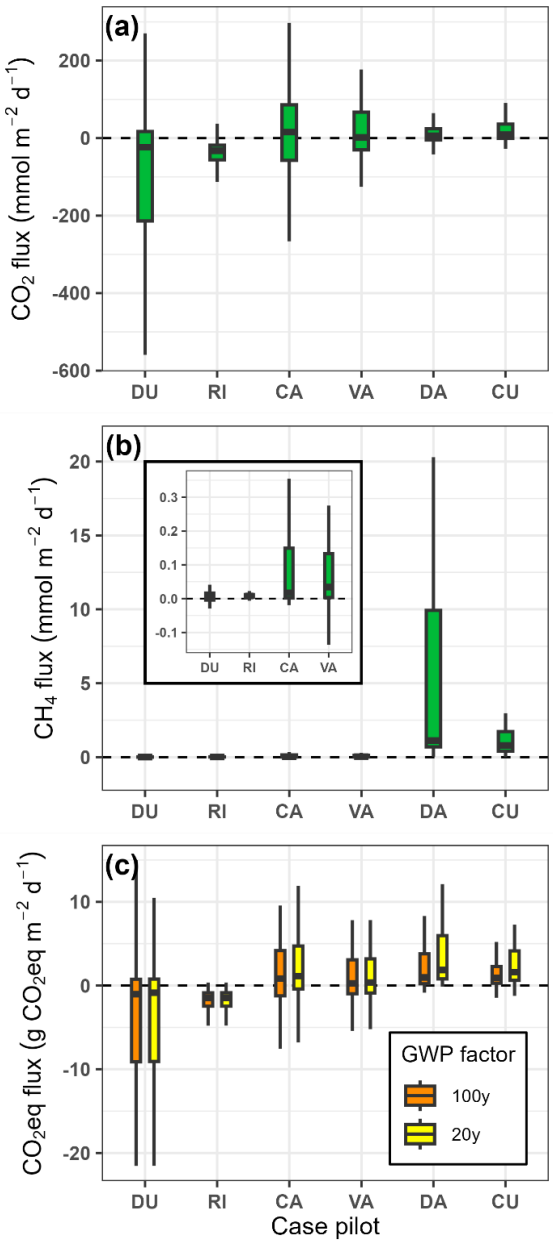

Figure 2. Greenhouse gas fluxes across preserved case pilot wetlands of (a) CO_2, (b) CH_4, and (c) combined CO_2-eq under 100y and 20y GWP scenarios. Boxplots show the median, interquartile range (IQR), and whiskers extending to 1.5xIQR; data outside these ranges are not displayed for clarity. Inset in (b) shows a zoomed-in view of CH_4 flux data for DU, RI, CA, and VA to better visualize differences; y-axis scale differs from the main panel.

3.2. Effect of conservation status on CO_2 fluxes

Daily CO_2 fluxes (mmol m^{-2} d^{-1}) showed wetland-specific patterns related to the conservation status (**Figure 3**). Significant status effects were detected in three case pilot wetlands (RI, DA, CU) (**Table S1**), with clear differences between preserved, altered, and restored sites (**Table S3**). In RI and DA, altered sites exhibited significantly higher CO_2 fluxes than preserved ($p \leq 0.002$) and restored ($p < 0.001$) sites, which showed similar low fluxes ($p = 0.71$) in RI while restored sites of DA showed slightly lower fluxes than preserved ones ($p = 0.042$). In contrast, CU displayed lower CO_2 fluxes in altered sites compared to preserved ($p < 0.001$) and restored ($p < 0.001$) sites. No statistically significant status effects were observed in DU, CA, or VA, where CO_2 fluxes were

comparable across conservation statuses ($p \geq 0.39$). Beyond status, CO_2 fluxes were consistently influenced by seasonality and vegetation presence, often interacting with the conservation status, even when status alone was not significant (**Table S1, Figures S3 and S6**). The three case pilot wetlands with significant conservation status effects on CO_2 fluxes (RI, DA, and CU) showed only minor increases from marginal to conditional R^2 values (**Table S1**), suggesting limited additional variance explained by the random site effect.

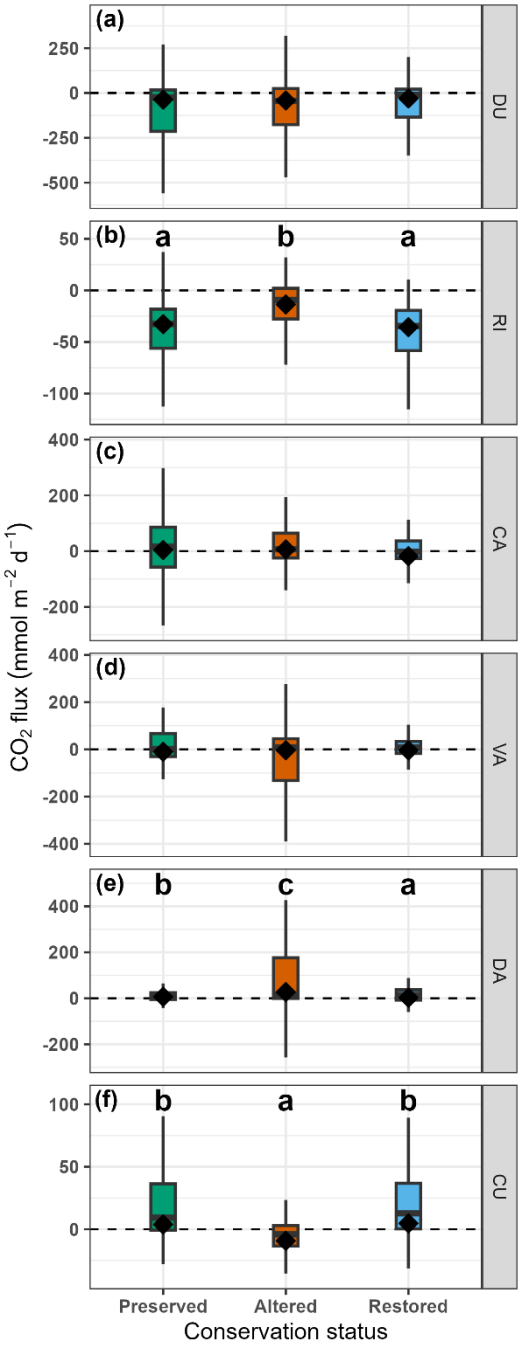

Figure 3. CO_2 fluxes (mmol m^{-2} d^{-1}) according to conservation status for each case pilot. Boxplots show the median, interquartile range (IQR), and whiskers extending to 1.5xIQR; data outside these ranges are not displayed for clarity. Diamonds represent estimated marginal means (EMMs) derived from parametric bootstrap distributions. Different letters indicate significant differences among EMMs based on empirical pairwise contrasts ($p < 0.05$; **Table S3**).

3.3. Effect of conservation status on CH_4 fluxes

CH_4 fluxes (mmol m^{-2} d^{-1}) showed clearer and more frequent statistically significant responses to conservation status across case pilot wetlands (**Figure 4**). Significant status effects were detected in all case pilot wetlands except DU (**Table S1**), where CH_4 fluxes did not differ among preserved, altered and restored sites (**Table S3**). In RI, preserved and restored sites exhibited slightly higher CH_4 fluxes than altered sites ($p = 0.006$, and $p < 0.001$, respectively). In the Mediterranean wetlands (CA and VA), altered sites showed higher CH_4 emissions than preserved sites ($p \leq 0.022$), with restored sites of CA showing fluxes similar to preserved sites ($p = 0.26$) and lower than altered ones ($p = 0.029$), while restored sites of VA showed intermediate fluxes not different from altered or preserved sites ($p > 0.35$). In DA, restored sites had higher CH_4 fluxes than altered sites ($p = 0.041$), while preserved sites were intermediate. In CU, altered sites exhibited substantially higher CH_4 emissions than both preserved and restored sites ($p < 0.001$), which showed similarly low fluxes. As for CO_2, CH_4 flux variability was strongly influenced by seasonality across all case pilots and by vegetation presence in most cases, with frequent interactions between the conservation status, season, and vegetation presence (**Table S1, Figures S4 and S7**). In contrast to CO_2 models, CH_4 models generally showed substantially higher conditional than marginal R^2 values (**Table S1**), indicating that site-level variability contributed importantly to model explanatory power, particularly in DA ($R^2m = 0.50$, $R^2c = 0.68$).

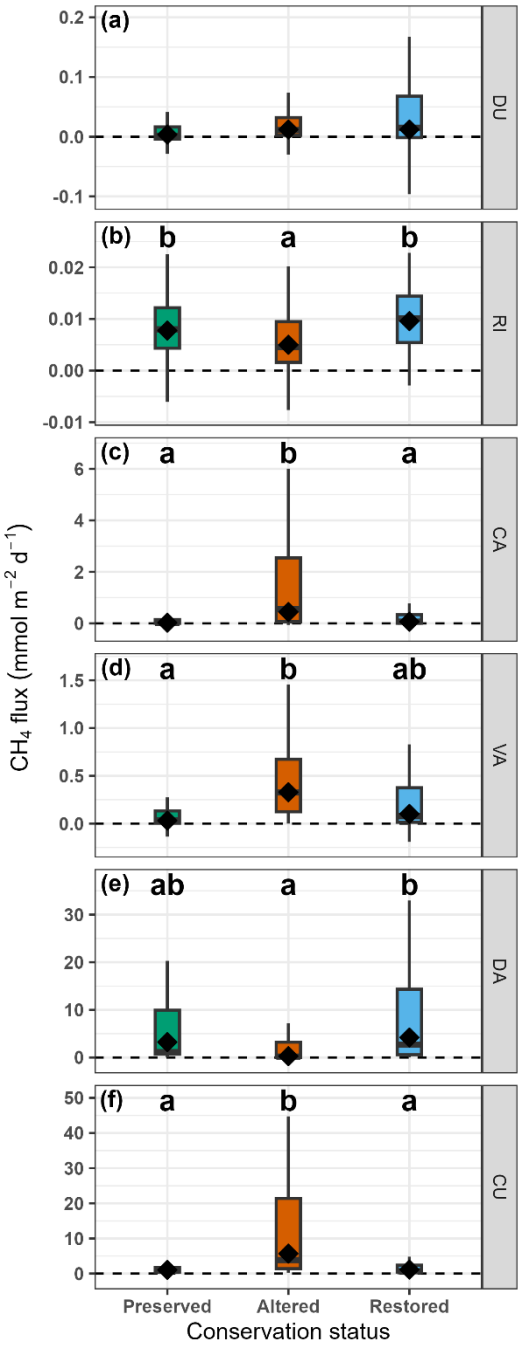

Figure 4. CH_4 fluxes (mmol m^{-2} d^{-1}) according to conservation status for each case pilot. Boxplots show the median, interquartile range (IQR), and whiskers extending to 1.5xIQR; data outside these ranges are not displayed for clarity. Diamonds represent estimated marginal means (EMMs) derived from parametric bootstrap distributions. Different letters indicate significant differences among EMMs based on empirical pairwise contrasts ($p < 0.05$; **Table S3**).

3.4. Effect of conservation status on CO_2-eq fluxes

The influence of conservation status on combined CO_2-eq fluxes (**Figure 5**) was assessed using pairwise comparisons of bootstrap CO_2-eq distributions under both 100-year and 20-year CH_4 GWP scaling factors (**Table S3**). In general, differences in CO_2-eq fluxes among conservation statuses were less consistent than those observed for CO_2 and CH_4 individually and depended on the selected GWP time horizon. The clearest status-related differences were observed for the RI

case pilot wetland, where restored and preserved sites consistently showed lower CO_2-eq fluxes than altered sites ($p \leq 0.002$), while not differing from each other ($p > 0.71$) under both 100-year and 20-year GWP scenarios. The only other wetland showing significant differences in CO_2-eq fluxes among conservation statuses was CU, although these differences were only detected under the 20-year GWP scenario. In CU, restored and preserved sites showed lower CO_2-eq fluxes than altered sites ($p \leq 0.006$), while remaining similar to each other ($p = 0.82$). Although the central distributions of CO_2-eq fluxes appeared to follow status-specific patterns in some wetlands (e.g., CA or DA), no statistically significant differences among conservation statuses were detected in these systems (**Table S3**). As observed for the individual CO_2 and CH_4 flux components, CO_2-eq fluxes also exhibited substantial variability that appeared associated with seasonality and vegetation presence (**Figures S5 and S8**), although these effects were not directly quantified for combined CO_2-eq metrics.

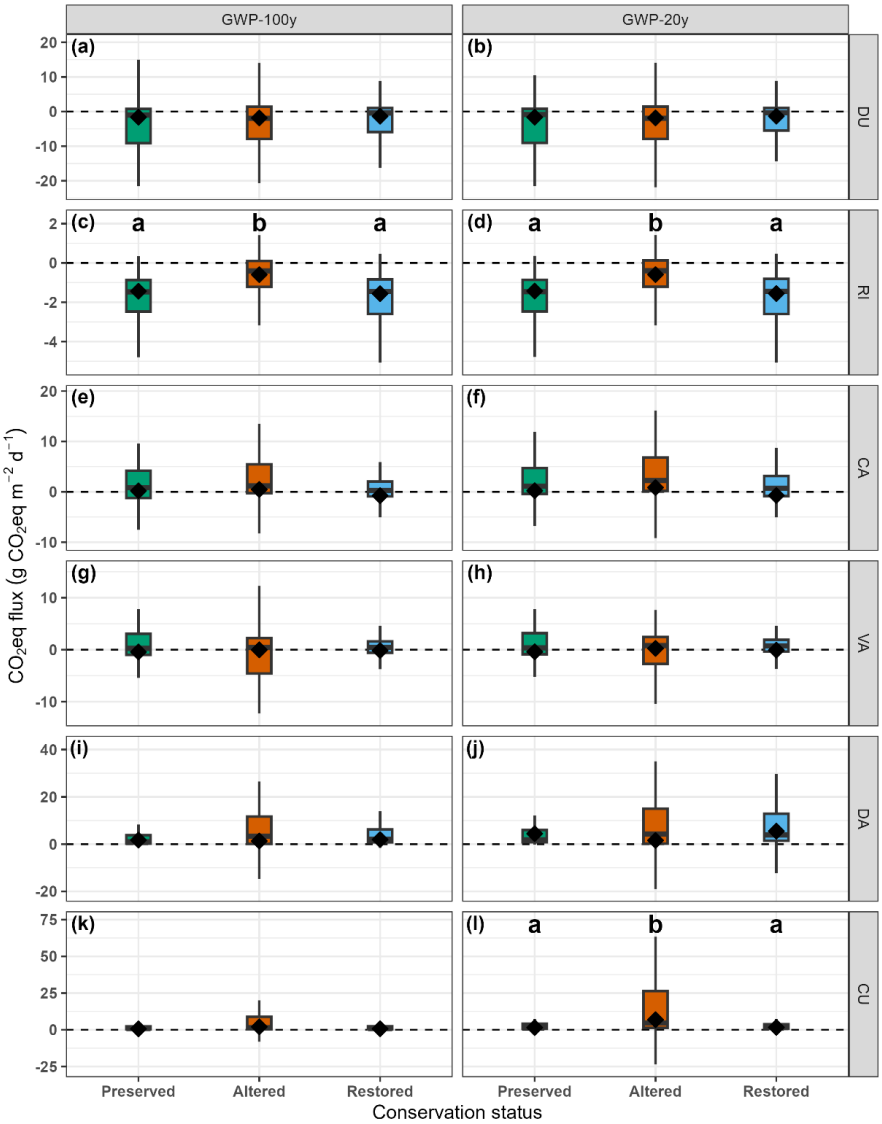

Figure 5. CO_2-eq flux (g CO_2 eq. m^{-2} d^{-1}) according to conservation status for each case pilot under 100y and 20y GWP scenarios. Boxplots show the median, interquartile range (IQR), and whiskers extending to 1.5xIQR; data outside these ranges are not displayed for clarity. Diamonds represent estimated marginal means (EMMs) derived from paired parametric bootstrap distributions of CO_2 and CH_4 models after application of the corresponding GWP factors. Different letters indicate significant differences among EMMs based on empirical pairwise contrasts ($p < 0.05$; **Table S3**).

4. Discussion

4.1. Biogeochemical drivers of gaseous C exchange in European coastal wetlands

Across the wetlands examined, the effects of conservation status on CO_2 and CH_4 fluxes varied among the studied wetland types, their specific alterations and associated restoration measures. CO_2 fluxes showed variations significantly associated with the conservation status in only three of six case pilots, whereas CH_4 fluxes were more responsive, with significant effects in five of six case pilots. Wherever status effects were detected for CO_2, they were consistently opposite in direction to those of CH_4, reflecting contrasting conditions that control the underlying processes regulating CO_2 and CH_4 exchanges in the different wetlands considered, with enhancement of aerobic conditions increasing CO_2 release, while actions favoring anaerobic conditions (e.g., rewetting) increased CH_4 emissions. Despite this variability, mostly depending on the specific features of each wetland type and the conservation status of sites, some common mechanisms were evident across wetland types.

The diversity of wetland types and ecological conditions examined allowed identification of key drivers of CO_2 and CH_4 exchanges, strongly modulated by seasonality. CO_2 fluxes were primarily controlled by vegetation cover and sediment oxygen availability, which regulated the balance between photosynthetic uptake and respiration-mediated release of CO_2. Emissions of CH_4 were mostly related to hydrology-driven oxygen availability in the sediment, salinity conditions, and presence of reed-type vegetation, while labile organic matter supply was important in some systems. CO_2 exchange responded mostly to alteration and restoration actions that severely modified the landscape of the wetlands, either through substantial loss or gain in abundance of primary producers or through profound changes in inundation patterns related to land-use change. CH_4 emissions were more sensitive to less evident hydrological changes, either through variations in water quality and salinity or through hydrodynamics modifying the extent and timing of wetlands flooding and water table depths. This sensitivity is strongly seasonal and temperature-driven, an effect that becomes increasingly evident at lower latitudes. Global changes that extend warm periods could potentially extend the duration of the observed seasonal CH_4 emission peaks in summer (Camacho et al., 2017; Morant et al., 2024); thus, accounting for seasonal variability is essential to accurately assess restoration outcomes, or the consequences of their absence.

Emergent vegetation presence exerted strong and consistent impact on CO_2 fluxes across all wetland types where it was evaluated, with vegetated areas generally acting as net CO_2 sinks (**Table S1**, **Figure S6**). This evidences that, although strongly regulated by seasonality and local climatic conditions, vegetation standing stock is a primary driver of ecosystem-level primary production through photosynthetic uptake of CO_2 (Reddy et al., 2022). While our statistical framework could not explicitly include this effect for the seagrass meadows of Ria de Aveiro, the expected stronger CO_2 uptake by *Zostera noltii* meadows with respect to bare mudflats becomes evident when considering the strong differences in vegetated coverage between the sites of different conservation status sampled. RI altered sites suffered from erosion, bait-digging and trampling (**Table 1**), which reduced their *Z. noltii* coverage to an average of 8%. Instead, preserved sites as well as restored sites after seagrass planting showed much higher average *Z. noltii* coverages (61% and 96%, respectively), which is the likely explanation behind the significantly enhanced CO_2 uptake shown by these sites (**Figure 3b**).

Plant community composition is also sometimes shown to influence overall CO_2 uptake rates in wetlands (Ward et al., 2009). Several of the wetlands studied suffered from alterations that involved modified vegetation communities such as presence of invasive species and loss of native vegetation and land use change (**Table 1**). Generally, the CO_2 exchange profile in vegetated areas of different conservation status did not reveal significant differences (**Figure S6**), indicating that environmental alterations related to shifts in plant community composition had little impact on CO_2 exchange in the studied wetlands. While vegetation composition is a good indicator of the overall ecological integrity of wetland systems, the potential biogeochemical effects of these types of shifts (Davidson et al., 2018) were not of sufficient magnitude to be detected in our study. Although the vegetated areas of the Danube Delta wetlands did show significant differences that might be associated with differences in primary productivity of reed stands and agricultural crop species (**Figure S6**), these coincided with permanently inundated substrates and agricultural soils, respectively. Thus, the observed differences likely arise from two main factors: differences in vegetation primary production efficiency and lower aerobic respiration rates due to oxygen limitation in submerged sediments and the water column compared with well-aerated agricultural soils (Bianchi et al., 2021). This interpretation is supported by the higher CO_2 emissions measured in non-vegetated areas of altered sites relative to preserved and restored sites in the Danube Delta (**Figure S6**). These two non-exclusive mechanisms likely resulted in the status-level differences in CO_2 fluxes observed in the Danube Delta (**Figure 3e**). Finally, the abundance of other primary producers (phytoplankton) appears to be the dominant driver responsible for the CO_2 exchange profiles observed in the Curonian Lagoon (**Figure 3f**). In this wetland, nutrient load was the main alteration factor related to conservation status and ecosystem interventions (**Table 1**), leading to eutrophication and associated massive phytoplankton blooms in altered sites (Vaičiūtė et al., 2021; Zilius et al., 2014), as indicated by water chlorophyll-a concentrations (**Table S4**). Thus, enhanced CO_2 uptake and reduced respiration under anoxic conditions driven by organic C accumulation by phytoplankton in open water areas (**Figure S6**) seem to be the main drivers behind the general status-level differences in CO_2 exchange profiles of the Curonian Lagoon (**Figure 3f**).

Hydrology emerged as a dominant control on CH_4 exchanges across the wetlands studied, with site inundation proportion (quantified as the percentage of chambers deployed in flooded areas) showing a clear positive relationship with CH_4 emissions across systems (**Figure S9**). Permanently flooded sediments promote anoxic conditions that favor methanogenesis (Camacho-Santamans et al., 2025; Rochera et al., 2025) while restricting aerobic respiration and thus CO_2 releases. This mechanism is exemplified by the general inter-wetland type variability observed for CH_4 (**Figure 2**), where well-preserved freshwater systems characterized by permanently flooded conditions and limited salinity constraints on methanogenesis (Camacho et al., 2017; Miralles-Lorenzo et al., 2025; Morant et al., 2024), such as Danube Delta lakes and the Curonian Lagoon, presented by far the largest emission profiles of CH_4. A similar pattern was observed for the freshwater marshes of Camargue, where wetland hydrology was a main determinant of the conservation status (**Table 1**) and CH_4 emissions (**Figure 4c**). The hydrodynamics of altered CA sites favored flooded conditions, as reflected by 73% of chamber deployments in these sites occurring in inundated areas with respect to 48% for preserved sites. Accordingly, altered sites presented overall higher CH_4 emissions (**Figure 4c**, **Table S3**), particularly during the summer season (**Figure S4**), coinciding with the highest discrepancy in flooded area proportion between altered and preserved sites (82% vs. 40%) and high temperatures that likely limited oxygen availability and enhanced microbial activity in submerged sediments (Cui et al., 2024). Modified hydrology was also an important factor regulating CH_4 emissions in the brackish Mediterranean marshes of

Marjal dels Moros, where similar differences in inundation proportion (65% vs 26%) were likely contributing to the higher CH_4 emissions observed in altered sites, with respect to preserved ones (**Figure 4d**). This strong hydrological control likely also explains why CH_4 models generally had larger differences between marginal and conditional R^2 values than CO_2 models (**Table S1**). Because fine-scale inundation variability was not explicitly represented in the fixed-effects structure, part of the hydrological variability regulating CH_4 production was likely absorbed by the random site effect, increasing its relative explanatory contribution. This pattern was particularly evident in the Danube Delta wetlands, where altered sites encompassed strongly contrasting hydrological conditions (**Supplementary Methods)**.

Nevertheless, CH_4 emissions were not only influenced by hydrology-driven oxygen availability of the sediments but also by salinity (electrical water conductivity), which showed a clear negative relationship with CH_4 emissions across wetlands (**Figure S10)**. Through the provision of sulfate as a more energetically favorable electron acceptor than CO_2, seawater intrusion regulates the dominance of sulfate-reducing over methanogenic microbes (Koebsch et al., 2019; Miralles-Lorenzo et al., 2025). This mechanism helps to explain the gradient in CH_4 emissions observed along the progressively more saline altered, restored and preserved sites of Marjal dels Moros (**Figure 4d**, **Table S4**). Additionally, this salinity-driven methanogenesis limitation in tidal wetlands such as DU saltmarshes and RI *Z. noltii* meadows is likely responsible for their extremely low CH_4 emissions with respect to the other coastal wetlands examined (**Figure 2**).

While anoxia and salinity help to regulate the dominant catabolic metabolism in sediments, the supply of different organic matter substrates is one of the principal factors regulating the overall rates of organic C degradation, and CH_4 emissions (Rissanen et al., 2023). Across the wetlands examined, the effect of labile organic matter supply in regulating CH_4 production can help to explain small but significantly higher CH_4 emissions of preserved and restored *Z. noltii* meadows with respect to bare altered sites of RI (**Figure 4b**), as seagrasses produce and release methylated compounds that represent an attractive substrate for methanogens (Schorn et al., 2022). Of more relevance is the pattern observed in the Curonian Lagoon wetland, where enhanced phytoplankton growth fueled by increased nutrient loads (**Table S4**) resulted in an accumulation of labile organic matter in the sediments of altered sites (Remeikaitė-Nikienė et al., 2016). Rapid degradation of phytoplankton-derived organic-C leads to anoxic conditions which, together with the freshwater character of the sites (Zilius et al., 2014), resulted in an ideal environment for methanogenesis, helping to explain the stark differences in CH_4 overall emissions between the altered and preserved and restored sites of this wetland (**Figure 4f**). Additionally, although these increased emissions of CU eutrophic sites were consistently detected in both open-water and vegetated areas, the magnitude of CH_4 emissions was much higher in reed-covered zones of CU, which is a common pattern observed across many of the wetlands examined (**Figure S7**). The consistently higher CH_4 emissions observed in vegetated zones likely result from vegetation-facilitated transfer of CH_4 from sediments to the atmosphere, bypassing oxidation in sediments and the water column (Ge et al., 2024). Ebullitive CH_4 transfer likely also contributed to the high variability observed in CH_4 fluxes, particularly in freshwater wetlands with high overall CH_4 emissions such as the Danube delta and Curonian Lagoon. Ebullition accelerates CH_4 transport to the atmosphere, limiting oxidation during water-column transit, but is also inherently variable over short temporal scales. Although ebullition was not independently quantified in this study, visual evidence of ebullitive dynamics was more prevalent in wetlands with higher CH_4 emissions, suggesting that this mechanism likely contributed to the elevated CH_4 fluxes and variability observed in these systems.

Importantly, the restoration actions examined across case pilots were not equivalent interventions applied across comparable systems, but rather context-specific responses to different forms of wetland alteration. Thus, comparisons of GHG fluxes among conservation statuses were made within each case pilot, rather than across them. Nevertheless, two non-exclusive mechanisms emerged as primary drivers of changes in GHG exchange across wetlands: shifts in areal habitat composition and changes in process rates within habitats. Major alterations and restoration actions can modify wetland structure to the point where entire habitats such as vegetated or open water areas are lost along with their biogeochemical functioning. The loss and replantation of seagrass beds in Ria de Aveiro or the land-use changes involving draining and rewetting of the Danube Delta wetlands are extreme examples of this mechanism. Conversely, subtler interventions that do not visually alter the ecosystem landscape can nonetheless shift underlying processes and result in significant impacts on biogeochemical process rates. The degradation and subsequent recovery of water quality in the Curonian Lagoon through regulation of nutrient-loads is a good example of this mechanism: while the composition of open water and reed beds habitats remained the same between altered and restored sites, their habitat-specific rates of CO_2 and CH_4 production and atmospheric exchange were significantly different (**Figures S6, S7**). While the above examples represent extremes of these two mechanisms, it is important to recognize the existence of a continuum between them. It is also important to acknowledge that no single habitat-specific "reference" rate exists for any natural process. In this context, seasonal variability regulates GHG fluxes through two pathways: temperature and physiological shifts alter habitat-specific process rates, while seasonal flooding dynamically redistributes the relative extent of open water, vegetated areas, and bare sediments within wetlands.

The contrasting sensitivities and drivers of CO_2 and CH_4 often led to opposite flux responses to the same environmental interventions, making CO_2-eq outcomes dependent on wetland-specific gas dominance. Three general response groups emerged. In tidal wetlands (Dutch Delta and Ria de Aveiro), constant seawater supply suppressed CH_4 emissions to the point that this gas only represented an average 6% and 4% of CO_2-eq exchanges (20-year GWP), respectively. In these wetlands, only vegetation-related interventions resulted in a significant impact on their climatic functionality, with changes in CO_2 fluxes outbalancing all detected variations in CH_4 emissions (regardless of GWP scaling). In seasonally inundated Mediterranean marshes (Camargue and Marjal dels Moros), CH_4 played a moderate role in their CO_2-eq fluxes (25% and 19%, respectively; 20-year GWP). In these wetlands, high CO_2 flux variability obscured detected changes in CH_4 emissions, leading to no significant differences in CO_2-eq fluxes (for both 100-year and 20-year GWP). In permanently flooded freshwater wetlands (Danube lakes and Curonian Lagoon), CH_4 represented a higher average proportion of the wetland GHG balance in terms of CO_2-eq (56% and 62%, respectively; 20-year GWP). In these wetlands, ecosystem interventions had clear but opposite effects for CO_2 and CH_4 exchanges, which only resulted in changes of combined CO_2-eq fluxes when CO_2 responses were of relatively low magnitude and outbalanced by strong CH_4 changes scaled with a 20-year GWP factor.

4.2. Climate change mitigation potential of coastal European wetland restoration and conservation

This study offers valuable insights into the potential of European coastal wetland restoration as a climate mitigation tool through the exemplary results obtained from six diverse pilot wetlands. Comparison of CO_2, CH_4 and CO_2-eq exchange balances between altered and restored sites

provide a quantitative estimate of the mitigation potential of restoration across different wetland types (**Table S3**).

Although the central distributions of daily net fluxes showed apparent reductions in GHG fluxes following restoration in several pilot wetlands (**Figures 3, 4, 5**), driven by significant effects of the conservation status (**Table S1**), high data variability precluded the detection of statistically significant mean flux reductions in some cases (**Table S3**). Across the pilot wetlands, statistically significant mitigation of CO_2 fluxes was only detected for the restoration of Ria de Aveiro seagrass meadows and Danube Delta freshwater lakes, likely driven by increased net primary production of seagrass relative to bare sediment areas and reduced organic C decomposition rates in freshwater lakes compared with agricultural land use, respectively. For CH_4 fluxes, statistically significant mitigation was only observed following water quality improvement in the Curonian Lagoon, while restoration of natural hydrodynamics in Camargue achieved marginal CH_4 reductions that approached statistical significance. When CO_2 and CH_4 were combined as CO_2-eq, significant mitigation potential was only detected for seagrass replantation in Ria de Aveiro under both 100-year and 20-year CH_4 warming scenarios and for re-oligotrophication in the Curonian Lagoon under the 20-year scenario. These different outcomes emphasize that the climate change mitigation effects of wetland restoration mediated by changes in GHG fluxes cannot be generalized across intervention types or ecosystems. Restoration actions target different system-specific degradation pathways and therefore can influence distinct biogeochemical controls on GHG exchange, resulting in climatic effects that are strongly dependent on ecosystem context.

The magnitude of potential mitigated emissions associated with the restoration interventions examined across the pilot wetlands, quantified as significant reductions in GHG fluxes using altered conditions as baseline (**Table S3**) and reported here as mean ± SE [CI95 range], were generally within the range reported for other nature-based solutions. Restoration of RI seagrass meadows reduced fluxes by -353 ± 108 [-567 to -145] g CO_2-eq m^{-2} y^{-1} considering only CO_2 fluxes, with minimal change when CH_4 fluxes were incorporated (-351 ± 108 [-565 to -144] g CO_2-eq m^{-2} y^{-1}; 20-year GWP). These reductions are comparable to the -73 and -154 g CO_2-eq m^{-2} y^{-1} reported by Oreska et al. (2020) for 12- and 15-year seagrass restoration projects, and fall within the range of the global average net sink estimated for seagrass systems by Rosentreter et al. (2023) of -592 ± 309 g CO_2-eq m^{-2} y^{-1} (mean ± SE), including CO_2 and CH_4 fluxes (100-year GWP). Restoration of CU substantially reduced CH_4 emissions, corresponding to mitigation potentials of -719 ± 319 [-1485 to -230] and -2124 ± 942 [-4381 to -679] g CO_2-eq m^{-2} y^{-1} under 100-year and 20-year GWP scenarios, respectively. However, these reductions were partially offset by increased CO_2 fluxes, such that significant mitigation of combined CO_2-eq fluxes was only detected under the 20-year GWP scenario (-1900 ± 942 [-4176 to -447] g CO_2-eq m^{-2} y^{-1}). This pattern contrasts with that of peatland rewetting described by Darusman et al. (2023), where reductions in CO_2 emissions of -522 ± 131 [-781 to -226] were partially offset by increased GWP20-CH_4 emissions of 349 ± 29 [262 to 407] g CO_2-eq m^{-2} y^{-1}. Nevertheless, the mitigation potential estimated for CU falls within the ranges reported by Bernal et al. (2018) for other ecosystem interventions over a 20-year period, including planted forests (-4070 to -450), agroforestry (-1560 to -1080), and mangrove restoration (-2310 to -670) g CO_2-eq m^{-2} y^{-1}. Finally, restoration of freshwater marshes in CA did not significantly affect CO_2 fluxes (**Table S1)**, but did significantly reduce CH_4 emissions, (Table S3). When considered independently, these CH_4 reductions corresponded to a maximum mitigation potential of -175 ± 122 [-496 to -20] g CO_2-eq m^{-2} y^{-1} under the 20-year GWP scenario. The contrasting outcomes between 100-year and 20-year CH_4 warming scenarios highlight how the perceived climatic effectiveness of wetland

restoration depends strongly on the temporal framework used to evaluate CO_2-eq exchanges. Thus, careful consideration of these scenarios should be made when assessing the climate mitigation potential associated with wetland restoration.

The results show mitigation potential for restoration of some types of degraded coastal European wetlands; however, the cumulative nature of GHG emissions must be considered. Even in cases where restoration completely reverts the biogeochemical functioning of a degraded wetland back to pristine conditions, the net effect must account for the time during which the wetland presented increased emissions incurring in a "recovery debt" (Moreno-Mateos et al., 2017). While the limited potential impact of restoration might appear discouraging, the same temporal consideration highlights the elevated and persistent costs of inaction and the necessity to avoid degradation of coastal wetlands in the first place. Differences in GHG profiles between preserved and degraded conditions revealed clear trends that demonstrate the climate change mitigation potential of maintaining coastal European wetlands in good conservation status (**Table S3**). Potentially avoided emissions through conservation were often of similar or greater magnitude than those estimated for restoration of RI and CU wetlands, while achieving statistical significance in more cases. For example, in Mediterranean marsh systems where conservation status did not significantly affect CO_2 fluxes (CA and VA), avoided CH_4 emissions through conservation exceeded those estimated for restoration and corresponded to mitigation potentials of up to -193 ± 121 [-511 to -46] and -139 ± 107 [-418 to -21] g CO_2-eq m^{-2} y^{-1}, respectively, under a 20-year GWP scenario. These patterns reveal fundamental differences in the functioning of well preserved and restored ecosystems.

Restoration projects guided by ecological restoration theory typically focus on alleviating pressures through passive restoration and reconstructing ecosystem structures to accelerate inherent functional recovery via active restoration (Palmer et al., 2016). However, even when restoration is well implemented, functional recovery often lags structural recovery due to slow reestablishment of natural biotic networks underpinning biogeochemical processes (Moreno-Mateos et al., 2012). Additionally, hysteretic dynamics in the face of ecosystem degradation and recovery may lead to trajectories favoring unintended alternative degraded states (Suding et al., 2004). Overall, the risks inherent to wetland restoration, recovery pathways and generally slow biogeochemical functional recovery emphasize the importance of preserving natural wetlands in a good conservation status.

Despite the differences shown above, conservation and restoration are complementary tools for climate mitigation and should not be viewed as alternative management strategies. Additionally, the climate change mitigation signals (GHG abatement) discussed here should be interpreted within the scope of the methodological approach employed, which quantified surface-atmosphere GHG exchanges over limited temporal windows and did not account for potential lateral GHG transport pathways (see Section 2.5). It is important to recognize that our current assessment of restoration-associated climate mitigation potential does not account for other biogeochemically relevant benefits, such as expansion of wetland extent or potential reductions of nitrous oxide (N_2O) emissions (Kasak et al., 2021; Leo et al., 2019), and represents only a snapshot of the functional recovery process likely to improve over time (Moreno-Mateos et al., 2017). Thus, the lack of statistically significant reductions in areal CO_2 and CH_4 exchanges reported in **Table S3** should not be interpreted as evidence that wetland restoration lacks climate mitigation benefits. Moreover, none of the restoration strategies implemented across the different wetlands examined targeted GHG mitigation as an explicit primary objective (Oliveira et al., 2026). Therefore, the detected effects on GHG exchanges can be considered as an

additional co-benefit of restoration alongside improvements in other ecosystem services such as biodiversity, water quality and flood risk mitigation (Meli et al., 2014; Singh et al., 2019; Wu et al., 2023). Ultimately, although the results show that restoration caused significant increases in emissions of either CO_2 or CH_4 in some wetlands, these were always accompanied by similar or greater changes in the opposite direction for the other GHG species studied. Therefore, when considering the combined CO_2-eq exchange patterns associated with restoration of degraded wetlands, the only significant effects detected were net reductions, indicating a net climatic cooling effect (**Table S3**).

This study highlights the diverse biogeochemical controls on GHG regulation across European coastal wetlands under different conservation statuses. These functional and site-specific differences must be explicitly considered in restoration and management planning to avoid trade-offs with other ecosystem services (Pörtner et al., 2021). Restoration strategies should therefore incorporate targeted, long-term monitoring to track wetland recovery and detect structural or functional deviations that require corrective action.

Wetlands have been heavily impacted by land-use change due to the historical undervaluation of their ecosystem services, often favoring higher-value uses despite substantial ecological losses (Zorrilla-Miras et al., 2014). This underscores the need to explore financing mechanisms that recognize the economic value of wetland ecosystem services, particularly their potential for climate mitigation. However, wetland climate mitigation capacity arises from complex, system-specific interactions among multiple GHGs, characterized by high spatial and temporal variability. Financing schemes should therefore be linked to comprehensive, long-term monitoring of all GHG fluxes relevant to the climatic functioning of each wetland system to avoid incomplete accounting and over-crediting risks prevalent in current carbon offset markets (Romm et al., 2025). Monitoring schemes should thus be guided by the understanding of each wetland's biogeochemical functioning while making use of standardized methodologies for fair monitoring, reporting and verification (Misteli et al., 2025). Given the strong seasonal variability observed across all wetlands examined, single annual measurements would likely be insufficient to characterize GHG dynamics robustly. However, in systems overwhelmingly dominated by CO_2 exchanges such as the RI seagrass meadows, monitoring resources could be prioritized toward measuring CO_2 over CH_4 fluxes and, if system functioning is sufficiently well understood, even toward proxies such as vegetation extent or biomass. Ultimately, for coastal wetland restoration to be an effective nature-based climate solution, projects must demonstrate additionality, feasibility, and permanence, and provide enough evidence to accurately quantify their climate benefits (Jones et al., 2024).

Currently, estimates of climate mitigation capacity of wetland restoration are highly variable (Griscom et al., 2017), stemming from incomplete understanding of several climate relevant processes. A common identified issue is the lack of widespread data on how GHG exchanges, in particular CH_4 and N_2O emissions, respond to coastal wetland restoration (Rosentreter et al., 2021). While the climatic effect of restoration projects in other ecosystems might be well represented by simple C balance assessments, in wetlands systems monitoring of these non-CO_2 GHG exchanges, and consideration of their time-horizon dependent warming effects is essential to accurately quantify net climatic impact (Macreadie et al., 2019). Transient increases in CH_4 emissions from restored wetlands can, considering radiative forcings and atmospheric lifetimes of GHGs, considerably delay climatic benefits of increased C storage (Schuster et al., 2024). Therefore, wetland restoration actions that achieve timely reductions of CH_4 emissions, such as those of Curonian Lagoon and to a lesser extent Camargue and Marjal dels Moros, become

especially relevant to meeting climatic mitigation targets. Additionally, the importance of lateral C and off-site GHG exchanges is increasingly being recognized, and future studies should therefore aim to obtain a more complete assessment of watershed-level budgets that support management decisions (Jones et al., 2024; Regnier et al., 2022). Finally, appropriate pre-restoration baseline reference condition measurements are essential to provide actionable knowledge to managers, thereby allowing quantification of actual benefits of alteration-specific reversals.

Given the ample and clear benefits of coastal wetland restoration on the provisioning of other ecosystem services, widespread restoration of degraded systems should nonetheless be pursued. We advocate taking advantage of recent policy momentum, exemplified by the EU Nature Restoration Regulation (Kampa et al., 2025), to gather more evidence on the effects of coastal wetland restoration on GHG exchange, enabling us to quantify more precisely the magnitude, consistency and reliability of potential associated climatic benefits.

5. Conclusions

This study examined how the conservation status and system-specific restoration actions of diverse European coastal wetlands influence atmospheric exchanges of CO_2 and CH_4 and their combined effects on climate forcing expressed as CO_2-eq. The results of this study show that GHG fluxes respond differently to degradation and restoration actions depending on the wetland type and associated main biogeochemical drivers. In particular, CO_2 fluxes responded primarily to landscape-scale changes in vegetation cover and inundation, whereas CH_4 exchanges were more sensitive to environmental modification and readily responded to less evident changes in water quality, salinity, and hydrodynamics.

These contrasting responses, together with the different relative contributions of CO_2 and CH_4 to net climatic forcing, translated into wetland-specific CO_2-eq exchange patterns associated with restoration and conservation. Replantation of seagrass meadows consistently emerged as an effective restoration measure associated with significant reductions in surface-atmosphere CO_2-eq exchanges under both 100-year and 20-year CH_4 warming scenarios, while eutrophication reversal through improved water treatment was associated with significant reductions under the 20-year scenario. Other actions, such as the reestablishment of natural salinity and hydrodynamics regimes, showed signs of reducing CH_4 emissions, but high CO_2 flux variability precluded detection of significant reductions in combined CO_2-eq emissions with the measured data.

While this study did not assess potential changes in N_2O emissions, the observed patterns for CO_2 and CH_4 contribute to the growing body of evidence supporting wetland restoration as a promising nature-based solution for climate change mitigation. At the same time, the findings of our study underscore the importance of considering multiple GHGs and their specific biogeochemistry when evaluating the climatic impact of wetland restoration projects. Further research should therefore aim to simultaneously quantify complete exchange budgets of CO_2, CH_4 and N_2O over management-relevant timeframes to better characterize the functional recovery process and obtain more complete assessments of the climatic implications associated with wetland restoration.

Within the scope of this study, restoration projects implemented across a range of European coastal wetland types showed no evidence of significant detrimental effects in terms of CO_2-eq. Instead, the results demonstrate that restoration was generally associated with maintained or improved CO_2-eq exchange profiles favoring climate change mitigation. Combined with ample evidence for other ecosystem service co-benefits, the results of our study support current regulatory efforts aimed at recovering historically degraded European wetlands while underscoring the need for targeted, ecosystem-specific restoration strategies to maximize potential climate mitigation benefits.

Acknowledgments

Funding for this research came from the project RESTORE4Cs - Modelling RESTORation of wEtlands for Carbon pathways, Climate Change mitigation and adaptation, ecosystem services, and biodiversity, Co-benefits (DOI: 10.3030/101056782), funded by the European Union under the Horizon Europe research and innovation programme (Grant Agreement ID: 101056782). The views and opinions expressed are those of the author(s) only and do not necessarily reflect those of the European Union or the granting authority. Neither the European Union nor the granting authority can be held responsible for them. We also acknowledge the support of FCT – Fundação para a Ciência e a Tecnologia I.P., to CESAM-Centro de Estudos do Ambiente e do Mar, under the project references UID/50017/2025 (doi.org/10.54499/UID/50017/2025) and LA/P/0094/2020 (doi.org/10.54499/LA/P/0094/2020). We thank Sara Ribeiro for logistical support. Work by the University of Valencia was also co-supported by projects CLIMAWET-CONS (PID2019-104742RB-I00), funded by the Agencia Estatal de Investigación of the Spanish Government, and by the project ECCAEL (PROMETEO CIPROM-2023-031), funded by the Generalitat Valenciana, both granted to Antonio Camacho. Dani von Schiller is a Serra Húnter Fellow.

Declaration of generative AI and AI-assisted technologies in the manuscript preparation process

During the preparation of this work the authors used ChatGPT-5.2 in order to identify potential improvements in text readability and for coding syntax support during data processing. After using this tool/service, the authors reviewed and edited the content as needed and take full responsibility for the content of the published article.

Data and code availability

Data presented in this article is deposited at LifeWatch ERIC (https://doi.org/10.48372/C29B-QW38) and will be fully accessible after December 31st, 2027. During the embargo period, data will be made available upon reasonable request. The code to reproduce the results of this article is archived at Zenodo (https://doi.org/10.5281/zenodo.21129514).

CRediT authorship contribution statement

Miguel Cabrera-Brufau: Writing – original draft, Visualization, Methodology, Investigation, Formal analysis, Data curation. **Camille Minaudo:** Writing – review & editing, Methodology, Investigation, Data curation. **Katrin Attermeyer:** Writing – review & editing, Methodology, Investigation, Conceptualization. **Alba Camacho-Santamans:** Writing – review & editing, Methodology, Investigation. **Rafael Carballeira:** Writing – review & editing, Methodology, Investigation. **Benjamin Misteli:** Writing – review & editing, Methodology, Investigation. **Jorge Montes-Pérez:** Writing – review & editing, Methodology, Investigation. **Daniel Morant:** Writing – review & editing, Methodology, Investigation. **Biel Obrador:** Writing – review & editing, Methodology, Investigation, Conceptualization. **Antonio Picazo:** Writing – review & editing, Methodology, Investigation. **Carlos Rochera:** Writing – review & editing, Methodology, Investigation. **Mihai Adamescu:** Writing – review & editing, Investigation. **Raquel Ambrosio:** Writing – review & editing, Investigation. **Giancarlo Bachi:** Writing – review & editing, Investigation. **Nina Bègue:** Writing – review & editing, Investigation. **Martynas Bučas:** Writing – review & editing, Investigation. **Lídia Cañas Ramírez:** Writing – review & editing, Methodology, Investigation. **Marco Carloni:** Writing – review & editing, Investigation. **Lamara Cavalcante:** Writing – review & editing, Investigation. **Constantin**

Cazacu: Writing – review & editing, Investigation. **Giovanni Checcucci:** Writing – review & editing, Investigation. **J. Pedro Coelho:** Writing – review & editing, Investigation. **Valentin Dinu:** Writing – review & editing, Investigation. **Valtere Evangelista:** Writing – review & editing, Investigation. **Ilenia Férez Martín:** Writing – review & editing, Methodology, Investigation. **Jonas Gintauskas:** Writing – review & editing, Investigation. **Relu Giuca:** Writing – review & editing, Investigation. **Anis Guelmami:** Writing – review & editing, Investigation. **Mirco Guerrazzi:** Writing – review & editing, Investigation. **Samuel Hilaire:** Writing – review & editing, Investigation. **Marija Kataržytė:** Writing – review & editing, Investigation. **Ana I. Lillebø:** Writing – review & editing, Project administration, Investigation, Funding acquisition, Conceptualization. **Raquel Lizán:** Writing – review & editing, Investigation. **Bruna R.F. Oliveira:** Writing – review & editing, Investigation. **Vitor H. Oliveira:** Writing – review & editing, Investigation. **Marta Pedrón:** Writing – review & editing, Investigation. **Jolita Petkuvienė:** Writing – review & editing, Investigation. **Tudor Racoviceanu:** Writing – review & editing, Investigation. **Michael Ronse:** Writing – review & editing, Investigation. **Chiara Santinelli:** Writing – review & editing, Investigation. **Ana I. Sousa:** Writing – review & editing, Investigation. **Wouter Suykerbuyk:** Writing – review & editing, Investigation. **Edvinas Tiškus:** Writing – review & editing, Investigation. **Claudia Tropea:** Writing – review & editing, Investigation. **Diana Vaičiūtė:** Writing – review & editing, Investigation. **Silvia Valsecchi:** Writing – review & editing, Investigation. **Marinka van Puijenbroek:** Writing – review & editing, Investigation. **Mourine J. Yegon:** Writing – review & editing, Investigation. **Antonio Camacho:** Writing – review & editing, Project administration, Methodology, Investigation, Funding acquisition, Conceptualization. **Daniel von Schiller:** Writing – review & editing, Project administration, Methodology, Investigation, Funding acquisition, Conceptualization.

References

Airoldi, L., Beck, M., 2007. Oceanography and Marine Biology, Oceanography and Marine Biology: An Annual Review. CRC Press. https://doi.org/10.1201/9781420050943

Bernal, B., Murray, L. T., & Pearson, T. R. H. (2018). Global carbon dioxide removal rates from forest landscape restoration activities. Carbon Balance and Management, 13(1), 22. https://doi.org/10.1186/s13021-018-0110-8

Bertolini, C., da Mosto, J., 2021. Restoring for the climate: a review of coastal wetland restoration research in the last 30 years. Restor Ecol 29, e13438. https://doi.org/10.1111/rec.13438

Bianchi, A., Larmola, T., Kekkonen, H., Saarnio, S., Lång, K., 2021. Review of Greenhouse Gas Emissions from Rewetted Agricultural Soils. Wetlands 41, 108. https://doi.org/10.1007/s13157-021-01507-5

Bonaglia, S., Cheung, H.L.S., Politi, T., Vybernaite-Lubiene, I., McKenzie, T., Santos, I.R., Zilius, M., 2025. Eutrophication and urbanization enhance methane emissions from coastal lagoons. Limnol Oceanogr Lett 10, 140–150. https://doi.org/10.1002/lol2.10430

Cabrera-Brufau, M., Minaudo, C., von Schiller, D., Obrador, B., Attermeyer, K., Camacho, A., 2025. Instantaneous fluxes of carbon dioxide (CO2) and methane (CH4) of six European coastal wetlands under different ecological status measured seasonally with static chambers [Data set]. LifeWatch ERIC. https://doi.org/10.48372/C29B-QW38

Cabrera-Brufau, M., Minaudo, C. (2026). MCabreraBrufau/Restore4Cs_GHG_chamber_fluxes: Static Chamber CO_2 and CH_4 Flux Calculation Workflow (RESTORE4Cs project) (v1.0.0). Zenodo. https://doi.org/10.5281/zenodo.19184152

Cabrera-Brufau, M., Minaudo, C., Attermeyer, K., Camacho-Santamans, A., Carballeira, R., Misteli, B., Montes-Pérez, J. J., Morant, D., Obrador, B., Picazo Mozo, A., Rochera, C., von Schiller, D., & Camacho, A. (2026). Raw GHG static chamber data of RESTORE4Cs project (CO2 and CH4 concentration time series and incubation details) [Data set]. Zenodo. https://doi.org/10.5281/zenodo.18803756

Camacho, A., Picazo, A., Rochera, C., Santamans, A., Morant, D., Miralles-Lorenzo, J., Castillo-Escrivà, A., 2017. Methane Emissions in Spanish Saline Lakes: Current Rates, Temperature and Salinity Responses, and Evolution under Different Climate Change Scenarios. Water (Basel) 9, 659. https://doi.org/10.3390/w9090659

Camacho-Santamans, A., Morant, D., Rochera, C., Picazo, A., Camacho, A., 2025. Towards an enhancement of the climate change mitigation capacity of inland saline shallow lakes through hydrological regime and vegetation management: a modelling approach. Water Int 50, 197–224. https://doi.org/10.1080/02508060.2024.2311997

Canadell, J.G., Monteiro, P.M.S., 2023. Global Carbon and Other Biogeochemical Cycles and Feedbacks, in: Climate Change 2021 – The Physical Science Basis. Cambridge University Press, pp. 673–816. https://doi.org/10.1017/9781009157896.007

Cui, S., Liu, P., Guo, H., Nielsen, C.K., Pullens, J.W.M., Chen, Q., Pugliese, L., Wu, S., 2024. Wetland hydrological dynamics and methane emissions. Commun Earth Environ 5, 470. https://doi.org/10.1038/s43247-024-01635-w

939 Darusman, T., Murdiyarso, D., Impron, & Anas, I. (2023). Effect of rewetting degraded peatlands
940 on carbon fluxes: a meta-analysis. Mitigation and Adaptation Strategies for Global Change,
941 28(3), 10. https://doi.org/10.1007/s11027-023-10046-9

942 Davidson, I.C., Cott, G.M., Devaney, J.L., Simkanin, C., 2018. Differential effects of biological
943 invasions on coastal blue carbon: A global review and meta-analysis. Glob Chang Biol 24,
944 5218–5230. https://doi.org/10.1111/gcb.14426

945 European Environment Agency, 2024. Europe's state of water 2024 – The need for improved
946 water resilience. Publications Office of the European Union.
947 https://doi.org/10.2800/02236

948 European Union, 2024. Regulation (EU) 2024/1991 of the European Parliament and of the
949 Council of 24 June 2024 on nature restoration and amending Regulation (EU) 2022/869.

950 Fluet-Chouinard, E., Stocker, B.D., Zhang, Z., Malhotra, A., Melton, J.R., Poulter, B., Kaplan, J.O.,
951 Goldewijk, K.K., Siebert, S., Minayeva, T., Hugelius, G., Joosten, H., Barthelmes, A., Prigent,
952 C., Aires, F., Hoyt, A.M., Davidson, N., Finlayson, C.M., Lehner, B., Jackson, R.B., McIntyre,
953 P.B., 2023. Extensive global wetland loss over the past three centuries. Nature 2023
954 614:7947 614, 281–286. https://doi.org/10.1038/s41586-022-05572-6

955 Ge, M., Korrensalo, A., Laiho, R., Kohl, L., Lohila, A., Pihlatie, M., Li, X., Laine, A.M., Anttila, J.,
956 Putkinen, A., Wang, W., Koskinen, M., 2024. Plant-mediated CH4 exchange in wetlands: A
957 review of mechanisms and measurement methods with implications for modelling. Science
958 of the Total Environment. https://doi.org/10.1016/j.scitotenv.2023.169662

959 Graves, S., Piepho, H.-P., with help from Sundar Dorai-Raj, L.S., 2024. multcompView:
960 Visualizations of Paired Comparisons.
961 https://doi.org/10.32614/CRAN.package.multcompView

962 Griscom, B.W., Adams, J., Ellis, P.W., Houghton, R.A., Lomax, G., Miteva, D.A., Schlesinger, W.H.,
963 Shoch, D., Siikamäki, J. V., Smith, P., Woodbury, P., Zganjar, C., Blackman, A., Campari, J.,
964 Conant, R.T., Delgado, C., Elias, P., Gopalakrishna, T., Hamsik, M.R., Herrero, M., Kiesecker,
965 J., Landis, E., Laestadius, L., Leavitt, S.M., Minnemeyer, S., Polasky, S., Potapov, P., Putz, F.E.,
966 Sanderman, J., Silvius, M., Wollenberg, E., Fargione, J., 2017. Natural climate solutions.
967 Proceedings of the National Academy of Sciences 114, 11645–11650.
968 https://doi.org/10.1073/pnas.1710465114

969 Hartig, F., 2024. DHARMa: Residual Diagnostics for Hierarchical (Multi-Level / Mixed) Regression
970 Models. https://doi.org/10.32614/CRAN.package.DHARMa

971 He, T., Ding, W., Cheng, X., Cai, Y., Zhang, Y., Xia, H., Wang, X., Zhang, J., Zhang, K., Zhang, Q.,
972 2024. Meta-analysis shows the impacts of ecological restoration on greenhouse gas
973 emissions. Nat Commun 15, 2668. https://doi.org/10.1038/s41467-024-46991-5

974 Hutchinson, G.L., Mosier, A.R., 1981. Improved Soil Cover Method for Field Measurement of
975 Nitrous Oxide Fluxes. Soil Science Society of America Journal 45, 311–316.
976 https://doi.org/10.2136/sssaj1981.03615995004500020017x

977 IPCC, 2023. Climate Change 2021 – The Physical Science Basis. Cambridge University Press,
978 Cambridge. https://doi.org/10.1017/9781009157896

Jones, S.F., Arias-Ortiz, A., Baldocchi, D., Eagle, M., Friess, D.A., Gore, C., Noe, G., Nolte, S., Oikawa, P., Paytan, A., Raw, J.L., Roberts, B.J., Rogers, K., Schutte, C., Stagg, C.L., Thorne, K.M., Ward, E.J., Windham-Myers, L., Yando, E.S., 2024. When and where can coastal wetland restoration increase carbon sequestration as a natural climate solution? Cambridge Prisms: Coastal Futures. https://doi.org/10.1017/cft.2024.14

Kampa, E., Elkina, E., Otero, M., 2025. Unlocking potential of coastal wetalnds in Europe: Integration into National Restoration Plans. Policy Brief. RESTORE4Cs project. https://www.restore4cs.eu/wp-content/uploads/2025/09/RESTORE4Cs_Policy-Brief-2_EN.pdf

Kasak, K., Espenberg, M., Anthony, T.L., Tringe, S.G., Valach, A.C., Hemes, K.S., Silver, W.L., Mander, Ü., Kill, K., McNicol, G., Szutu, D., Verfaillie, J., Baldocchi, D.D., 2021. Restoring wetlands on intensive agricultural lands modifies nitrogen cycling microbial communities and reduces N2O production potential. J Environ Manage 299, 113562. https://doi.org/10.1016/j.jenvman.2021.113562

Koebsch, F., Winkel, M., Liebner, S., Liu, B., Westphal, J., Schmiedinger, I., Spitzy, A., Gehre, M., Jurasinski, G., Köhler, S., Unger, V., Koch, M., Sachs, T., Böttcher, M.E., 2019. Sulfate deprivation triggers high methane production in a disturbed and rewetted coastal peatland. Biogeosciences 16, 1937–1953. https://doi.org/10.5194/bg-16-1937-2019

Lenth, R. V, 2025. emmeans: Estimated Marginal Means, aka Least-Squares Means. https://doi.org/10.32614/CRAN.package.emmeans

Leo, K.L., Gillies, C.L., Fitzsimons, J.A., Hale, L.Z., Beck, M.W., 2019. Coastal habitat squeeze: A review of adaptation solutions for saltmarsh, mangrove and beach habitats. Ocean Coast Manag 175, 180–190. https://doi.org/10.1016/j.ocecoaman.2019.03.019

Lin, C.-W., Lin, W.-J., Ho, C.-W., Kao, Y.-C., Yong, Z.-J., Lin, H.-J., 2024. Flushing emissions of methane and carbon dioxide from mangrove soils during tidal cycles. Science of The Total Environment 919, 170768. https://doi.org/10.1016/j.scitotenv.2024.170768

Lorke, A., Bodmer, P., Noss, C., Alshboul, Z., Koschorreck, M., Somlai-Haase, C., Bastviken, D., Flury, S., McGinnis, D.F., Maeck, A., Müller, D., Premke, K., 2015. Technical note: drifting versus anchored flux chambers for measuring greenhouse gas emissions from running waters. Biogeosciences 12, 7013–7024. https://doi.org/10.5194/bg-12-7013-2015

Lovley, D.R., Klug, M.J., 1983. Sulfate Reducers Can Outcompete Methanogens at Freshwater Sulfate Concentrations. Appl Environ Microbiol 45, 187–192. https://doi.org/10.1128/aem.45.1.187-192.1983

Macreadie, P.I., Anton, A., Raven, J.A., Beaumont, N., Connolly, R.M., Friess, D.A., Kelleway, J.J., Kennedy, H., Kuwae, T., Lavery, P.S., Lovelock, C.E., Smale, D.A., Apostolaki, E.T., Atwood, T.B., Baldock, J., Bianchi, T.S., Chmura, G.L., Eyre, B.D., Fourqurean, J.W., Hall-Spencer, J.M., Huxham, M., Hendriks, I.E., Krause-Jensen, D., Laffoley, D., Luisetti, T., Marbà, N., Masque, P., McGlathery, K.J., Megonigal, J.P., Murdiyarso, D., Russell, B.D., Santos, R., Serrano, O., Silliman, B.R., Watanabe, K., Duarte, C.M., 2019. The future of Blue Carbon science. Nat Commun 10, 3998. https://doi.org/10.1038/s41467-019-11693-w

Maes, J., Teller, A., Erhard, M., Condé, S., Vallecillo, S., Barredo, J.I., Luisa, M., Malak, D.A., Trombetti, M., Vigiak, O., Zulian, G., Addamo, A.M., Grizzetti, B., Somma, F., Hagyo, A., Vogt,

P., Polce, C., Jones, A., Marin, A.I., Ivits, E., Mauri, A., Rega, C., Czúcz, B., Ceccherini, G., Pisoni, E., Ceglar, A., Palma, P. De, Cerrani, I., Meroni, M., Caudullo, G., Lugato, E., Vogt, J. V, Spinoni, J., Cammalleri, C., Bastrup-birk, A., Miguel, J.S., Román, S.S., Kristensen, P., Christiansen, T., Roo, A. De, Cardoso, A.C., Pistocchi, A., Del, I., Alvarellos, B., Tsiamis, K., Gervasini, E., Deriu, I., Notte, A. La, Viñas, R.A., Vizzarri, M., Camia, A., Kakoulaki, G., Bendito, E.G., Panagos, P., Ballabio, C., Scarpa, S., Orgiazzi, A., Ugalde, O.F., Santos-martín, F., 2020. Mapping and Assessment of Ecosystems and their Services : An EU ecosystem assessment. Ispra. https://doi.org/10.2760/757183

Maier, M., Weber, T.K.D., Fiedler, J., Fuß, R., Glatzel, S., Huth, V., Jordan, S., Jurasinski, G., Kutzbach, L., Schäfer, K., Weymann, D., Hagemann, U., 2022. Introduction of a guideline for measurements of greenhouse gas fluxes from soils using non-steady-state chambers. Journal of Plant Nutrition and Soil Science 185, 447–461. https://doi.org/10.1002/jpln.202200199

McGillycuddy, M., Warton, D.I., Popovic, G., Bolker, B.M., 2025. Parsimoniously Fitting Large Multivariate Random Effects in glmmTMB. J Stat Softw 112, 1–19. https://doi.org/10.18637/jss.v112.i01

Meli, P., Rey Benayas, J.M., Balvanera, P., Martínez Ramos, M., 2014. Restoration Enhances Wetland Biodiversity and Ecosystem Service Supply, but Results Are Context-Dependent: A Meta-Analysis. PLoS One 9, e93507. https://doi.org/10.1371/journal.pone.0093507

Minaudo, C., von Schiller, D., Misteli, B., Morant, D., Adamescu, M., Attermeyer, K., Basset, A., Carballeira, R., Cazacu, C., Coelho, J.P., Guelmami, A., Hilaire, S., Miralles, J., Obrador, B., Petkuviene, J., Picazo, A., Rochera, C., Santinelli, C., Teixeira, H., Titocci, J., Vaicute, D., Camacho, A., 2023. Methodological manual. Deliverable D4.2 Horizon RESTORE4Cs Project GA ID: 101056782.

Minaudo, C., Cabrera-Brufau, M., Montes-Pérez, J. J., Attermeyer, K., Camacho, A., Camacho-Santamans, A., Cazacu, C., Giuca, R., Lillebø, A., Misteli, B., Morant, D., Obrador, B., Oliveira, B. R. F., Petkuviené, J., Mozo, A. P., Rochera, C., & von Schiller, D. (2026). Uncertainty in aquatic greenhouse gas flux estimates arises from subjective processing of floating chamber time series. Limnology and Oceanography: Methods, 2026, e70054. https://doi.org/10.1002/lom3.70054

Miralles-Lorenzo, J., Picazo, A., Rochera, C., Morant, D., Casamayor, E.O., Menéndez-Serra, M., Camacho, A., 2025. Environmental Gradients and Conservation Status Determine the Structure and Carbon-Related Metabolic Potential of the Prokaryotic Communities of Mediterranean Inland Saline Shallow Lakes. Ecol Evol 15, e71286. https://doi.org/10.1002/ece3.71286

Misteli, B., Morant, D., Camacho, A., Adamo, M., Bachi, G., Bègue, N., Bučas, M., Cabrera-Brufau, M., Carballeira, R., Cavalcante, L., Cazacu, C., Coelho, J., Doebke, C., Dinu, V., Guelmami, A., Giuca, R., Kataržytė, M., Lillebø, A., Marin, A., Marangi, C., Minaudo, C., Montes-Pérez, J., Obrador, B., Oliveira, B., Petkuvienė, J., Picazo, A., van Puijenbroek, M., Ronse, M., Rochera, C., Sánchez, A., Santinelli, C., Sousa, A., von Schiller, D., Attermeyer, K., Tropea, C., Vaičiūtė, D., 2025. Coastal Wetland Restoration and Greenhouse Gas Pathways: A Global Meta-Analysis. EarthArXiv preprint. https://doi.org/10.31223/X51B39

Misteli, B., Attermeyer, K., Rochera, C., Lillebø, A.I., Camacho, A. 2025. How can coastal wetland restoration mitigate climate change? What we know and what is still unclear. Policy Brief. Restore4Cs project. https://www.restore4cs.eu/wp-content/uploads/2025/12/EN_Policy-Brief-9-v7_Final-1.pdf

Mitsch, W.J., Bernal, B., Nahlik, A.M., Mander, Ü., Zhang, L., Anderson, C.J., Jørgensen, S.E., Brix, H., 2013. Wetlands, carbon, and climate change. Landsc Ecol 28, 583–597. https://doi.org/10.1007/s10980-012-9758-8

Morant, D., Picazo, A., Rochera, C., Santamans, A.C., Miralles-Lorenzo, J., Camacho, A., 2020a. Influence of the conservation status on carbon balances of semiarid coastal Mediterranean wetlands. Inland Waters 10, 453–467. https://doi.org/10.1080/20442041.2020.1772033

Morant, D., Picazo, A., Rochera, C., Santamans, A.C., Miralles-Lorenzo, J., Camacho-Santamans, A., Ibañez, C., Martínez-Eixarch, M., Camacho, A., 2020b. Carbon metabolic rates and GHG emissions in different wetland types of the Ebro Delta. PLoS One 15, e0231713. https://doi.org/10.1371/journal.pone.0231713

Morant, D., Rochera, C., Picazo, A., Miralles-Lorenzo, J., Camacho-Santamans, A., Camacho, A., 2024. Ecological status and type of alteration determine the C-balance and climate change mitigation capacity of Mediterranean inland saline shallow lakes. Sci Rep 14, 29065. https://doi.org/10.1038/s41598-024-79578-7

Moreno-Mateos, D., Barbier, E.B., Jones, P.C., Jones, H.P., Aronson, J., López-López, J.A., McCrackin, M.L., Meli, P., Montoya, D., Rey Benayas, J.M., 2017. Anthropogenic ecosystem disturbance and the recovery debt. Nature Communications 2017 8:1 8, 14163-. https://doi.org/10.1038/ncomms14163

Moreno-Mateos, D., Power, M.E., Comín, F.A., Yockteng, R., 2012. Structural and Functional Loss in Restored Wetland Ecosystems. PLoS Biol 10, e1001247. https://doi.org/10.1371/journal.pbio.1001247

Neubauer, S.C., 2021. Global Warming Potential Is Not an Ecosystem Property. Ecosystems 24, 2079–2089. https://doi.org/10.1007/s10021-021-00631-x

O'Connor, J.J., Fest, B.J., Sievers, M., Swearer, S.E., 2020. Impacts of land management practices on blue carbon stocks and greenhouse gas fluxes in coastal ecosystems—A meta-analysis. Glob Chang Biol 26, 1354–1366. https://doi.org/10.1111/gcb.14946

Oliveira, B. R. F., Camacho, A., Guelmami, A., Schroder, C., Bègue, N., Bučas, M., Cazacu, C., Ciravegna, E., Coelho, J. P., Constantin, R. G., Hilaire, S., Kataržytė, M., Morant, D., Picazo, A., Polman, N., van Puijenbroek, M., Raoult, J., Rochera, C., Ronse, M., … Lillebø, A. I. (2026). European coastal wetlands datasets and their use in decision-support tools for policy restoration objectives. Environmental Science & Policy, 179, 104386. https://doi.org/10.1016/j.envsci.2026.104386

Oreska, M. P. J., McGlathery, K. J., Aoki, L. R., Berger, A. C., Berg, P., & Mullins, L. (2020). The greenhouse gas offset potential from seagrass restoration. Scientific Reports, 10(1), 7325. https://doi.org/10.1038/s41598-020-64094-1

Palmer, M.A., Zedler, J.B., Falk, D.A., 2016. Ecological Theory and Restoration Ecology. Foundations of Restoration Ecology: Second Edition 3–26. https://doi.org/10.5822/978-1-61091-698-1_1

Peterson, R.A., 2021. Finding Optimal Normalizing Transformations via bestNormalize. R J 13, 310–329. https://doi.org/10.32614/RJ-2021-041

Pörtner, H.-O., Scholes, R.J., Agard, J., Archer, E., Arneth, A., Bai, X., Barnes, D., Burrows, M., Chan, L., Cheung, W.L. (William), Diamond, S., Donatti, C., Duarte, C., Eisenhauer, N., Foden, W., Gasalla, M.A., Handa, C., Hickler, T., Hoegh-Guldberg, O., Ichii, K., Jacob, U., Insarov, G., Kiessling, W., Leadley, P., Leemans, R., Levin, L., Lim, M., Maharaj, S., Managi, S., Marquet, P.A., McElwee, P., Midgley, G., Oberdorff, T., Obura, D., Osman Elasha, B., Pandit, R., Pascual, U., Pires, A.P.F., Popp, A., Reyes-García, V., Sankaran, M., Settele, J., Shin, Y.-J., Sintayehu, D.W., Smith, P., Steiner, N., Strassburg, B., Sukumar, R., Trisos, C., Val, A.L., Wu, J., Aldrian, E., Parmesan, C., Pichs-Madruga, R., Roberts, D.C., Rogers, A.D., Díaz, S., Fischer, M., Hashimoto, S., Lavorel, S., Wu, N., Ngo, H., 2021. Scientific outcome of the IPBES-IPCC co-sponsored workshop on biodiversity and climate change. https://doi.org/10.5281/ZENODO.5101125

R Core Team, 2025. R: A Language and Environment for Statistical Computing.

Ramsar Convention, 1971. Convention on Wetlands of International Importance especially as Waterfowl Habitat. Ramsar.

Reddy, K.R., DeLaune, R.D., Inglett, P.W., 2022. Biogeochemistry of Wetlands, Biogeochemistry of Wetlands. CRC Press, Boca Raton. https://doi.org/10.1201/9780429155833

Regnier, P., Resplandy, L., Najjar, R.G., Ciais, P., 2022. The land-to-ocean loops of the global carbon cycle. Nature 603, 401–410. https://doi.org/10.1038/s41586-021-04339-9

Remeikaitė-Nikienė, N., Lujanienė, G., Malejevas, V., Barisevičiūtė, R., Žilius, M., Garnaga-Budrė, G., Stankevičius, A., 2016. Distribution and sources of organic matter in sediments of the south-eastern Baltic Sea. Journal of Marine Systems 157, 75–81. https://doi.org/10.1016/j.jmarsys.2015.12.011

Rheault, K., Christiansen, J.R., Larsen, K.S., 2024. goFlux: A user-friendly way to calculate GHG fluxes yourself, regardless of user experience. J Open Source Softw 9, 6393. https://doi.org/10.21105/joss.06393

Rissanen, A.J., Jilbert, T., Simojoki, A., Mangayil, R., Aalto, S.L., Khanongnuch, R., Peura, S., Jäntti, H., 2023. Organic matter lability modifies the vertical structure of methane-related microbial communities in lake sediments. Microbiol Spectr 11. https://doi.org/10.1128/spectrum.01955-23

Rochera, C., Picazo, A., Morant, D., Miralles-Lorenzo, J., Sánchez-Ortega, V., Camacho, A., 2025. Linking Carbon Fluxes to Flooding Gradients in Sediments of Mediterranean Wetlands. ACS ES&T Water 5, 2882–2890. https://doi.org/10.1021/acsestwater.4c00940

Romm, J., Lezak, S., Alshamsi, A., 2025. Are Carbon Offsets Fixable? Annu Rev Environ Resour 50, 649–680. https://doi.org/10.1146/annurev-environ-112823-064813

Rosentreter, J.A., Al-Haj, A.N., Fulweiler, R.W., Williamson, P., 2021. Methane and Nitrous Oxide Emissions Complicate Coastal Blue Carbon Assessments. Global Biogeochem Cycles 35, e2020GB006858. https://doi.org/10.1029/2020GB006858

Rosentreter, J. A., Laruelle, G. G., Bange, H. W., Bianchi, T. S., Busecke, J. J. M., Cai, W.-J., Eyre, B. D., Forbrich, I., Kwon, E. Y., Maavara, T., Moosdorf, N., Najjar, R. G., Sarma, V. V. S. S., van

Dam, B., & Regnier, P. (2023). Coastal vegetation and estuaries are collectively a greenhouse gas sink. Nature Climate Change, 13(6), 579–587. https://doi.org/10.1038/s41558-023-01682-9

Sadat-Noori, M., Andersen, M. S., Rutlidge, H., & Glamore, W. (2025). Coastal Wetland Restoration Effects on Carbon Dynamics: A Groundwater Perspective. Reviews of Geophysics, 63(3), e2025RG000895. https://doi.org/10.1029/2025RG000895

Saunois, M., Bousquet, P., Poulter, B., Peregon, A., Ciais, P., Canadell, J.G., Dlugokencky, E.J., Etiope, G., Bastviken, D., Houweling, S., Janssens-Maenhout, G., Tubiello, F.N., Castaldi, S., Jackson, R.B., Alexe, M., Arora, V.K., Beerling, D.J., Bergamaschi, P., Blake, D.R., Brailsford, G., Brovkin, V., Bruhwiler, L., Crevoisier, C., Crill, P., Covey, K., Curry, C., Frankenberg, C., Gedney, N., Höglund-Isaksson, L., Ishizawa, M., Ito, A., Joos, F., Kim, H.-S., Kleinen, T., Krummel, P., Lamarque, J.-F., Langenfelds, R., Locatelli, R., Machida, T., Maksyutov, S., McDonald, K.C., Marshall, J., Melton, J.R., Morino, I., Naik, V., O'Doherty, S., Parmentier, F.-J.W., Patra, P.K., Peng, C., Peng, S., Peters, G.P., Pison, I., Prigent, C., Prinn, R., Ramonet, M., Riley, W.J., Saito, M., Santini, M., Schroeder, R., Simpson, I.J., Spahni, R., Steele, P., Takizawa, A., Thornton, B.F., Tian, H., Tohjima, Y., Viovy, N., Voulgarakis, A., van Weele, M., van der Werf, G.R., Weiss, R., Wiedinmyer, C., Wilton, D.J., Wiltshire, A., Worthy, D., Wunch, D., Xu, X., Yoshida, Y., Zhang, B., Zhang, Z., Zhu, Q., 2016. The global methane budget 2000–2012. Earth Syst Sci Data 8, 697–751. https://doi.org/10.5194/essd-8-697-2016

Schorn, S., Ahmerkamp, S., Bullock, E., Weber, M., Lott, C., Liebeke, M., Lavik, G., Kuypers, M.M.M., Graf, J.S., Milucka, J., 2022. Diverse methylotrophic methanogenic archaea cause high methane emissions from seagrass meadows. Proceedings of the National Academy of Sciences 119. https://doi.org/10.1073/pnas.2106628119

Schuster, L., Taillardat, P., Macreadie, P.I., Malerba, M.E., 2024. Freshwater wetland restoration and conservation are long-term natural climate solutions. Science of The Total Environment 922, 171218. https://doi.org/10.1016/j.scitotenv.2024.171218

Schutte, C. A., Moore, W. S., Wilson, A. M., & Joye, S. B. (2020). Groundwater-Driven Methane Export Reduces Salt Marsh Blue Carbon Potential. Global Biogeochemical Cycles, 34(10), e2020GB006587. https://doi.org/10.1029/2020GB006587

Singh, N.K., Gourevitch, J.D., Wemple, B.C., Watson, K.B., Rizzo, D.M., Polasky, S., Ricketts, T.H., 2019. Optimizing wetland restoration to improve water quality at a regional scale. Environmental Research Letters 14, 064006. https://doi.org/10.1088/1748-9326/ab1827

Suding, K.N., Gross, K.L., Houseman, G.R., 2004. Alternative states and positive feedbacks in restoration ecology. Trends Ecol Evol 19, 46–53. https://doi.org/10.1016/j.tree.2003.10.005

Taillardat, P., Thompson, B.S., Garneau, M., Trottier, K., Friess, D.A., 2020. Climate change mitigation potential of wetlands and the cost-effectiveness of their restoration. Interface Focus 10, 20190129. https://doi.org/10.1098/rsfs.2019.0129

Thieurmel, B., Elmarhraoui, A., 2022. suncalc: Compute Sun Position, Sunlight Phases, Moon Position and Lunar Phase. https://doi.org/10.32614/CRAN.package.suncalc

Vaičiūtė, D., Bučas, M., Bresciani, M., Dabulevičienė, T., Gintauskas, J., Mėžinė, J., Tiškus, E., Umgiesser, G., Morkūnas, J., De Santi, F., Bartoli, M., 2021. Hot moments and hotspots of

cyanobacteria hyperblooms in the Curonian Lagoon (SE Baltic Sea) revealed via remote sensing-based retrospective analysis. Science of The Total Environment 769, 145053. https://doi.org/10.1016/j.scitotenv.2021.145053

Ward, S.E., Bardgett, R.D., McNamara, N.P., Ostle, N.J., 2009. Plant functional group identity influences short-term peatland ecosystem carbon flux: evidence from a plant removal experiment. Funct Ecol 23, 454–462. https://doi.org/10.1111/j.1365-2435.2008.01521.x

Wickham, H., 2016. ggplot2: Elegant Graphics for Data Analysis. Springer-Verlag New York.

Wickham, H., Pedersen, T.L., Seidel, D., 2025. scales: Scale Functions for Visualization. https://doi.org/10.32614/CRAN.package.scales

Wik, M., Crill, P. M., Varner, R. K., & Bastviken, D. (2013). Multiyear measurements of ebullitive methane flux from three subarctic lakes. Journal of Geophysical Research: Biogeosciences, 118(3), 1307–1321. https://doi.org/10.1002/jgrg.20103

Wu, Y., Sun, J., Hu, B., Zhang, G., Rousseau, A.N., 2023. Wetland-based solutions against extreme flood and severe drought: Efficiency evaluation of risk mitigation. Clim Risk Manag 40, 100505. https://doi.org/10.1016/j.crm.2023.100505

Zilius, M., Bartoli, M., Bresciani, M., Katarzyte, M., Ruginis, T., Petkuviene, J., Lubiene, I., Giardino, C., Bukaveckas, P.A., de Wit, R., Razinkovas-Baziukas, A., 2014. Feedback Mechanisms Between Cyanobacterial Blooms, Transient Hypoxia, and Benthic Phosphorus Regeneration in Shallow Coastal Environments. Estuaries and Coasts 37, 680–694. https://doi.org/10.1007/s12237-013-9717-x

Zorrilla-Miras, P., Palomo, I., Gómez-Baggethun, E., Martín-López, B., Lomas, P.L., Montes, C., 2014. Effects of land-use change on wetland ecosystem services: A case study in the Doñana marshes (SW Spain). Landsc Urban Plan 122, 160–174. https://doi.org/10.1016/j.landurbplan.2013.09.013

Supplementary materials for: Assessing the effects of restoration and conservation on gaseous carbon fluxes and climate mitigation potential across six European coastal wetlands

Miguel Cabrera-Brufau*[a], Camille Minaudo[a], Katrin Attermeyer[b], Alba Camacho-Santamans[a], Rafael Carballeira[c], Benjamin Misteli[b], Jorge Montes-Pérez[a], Daniel Morant[c], Biel Obrador[a], Antonio Picazo[c], Carlos Rochera[c], Mihai Adamescu[d], Raquel Ambrosio[e], Giancarlo Bachi[f], Nina Bègue[e], Martynas Bučas[g], Lídia Cañas Ramírez[a], Marco Carloni[f], Lamara Cavalcante[h], Constantin Cazacu[d], Giovanni Checcucci[f], J. Pedro Coelho[h], Valentin Dinu[d], Valtere Evangelista[f], Ilenia Férez Martín[a], Jonas Gintauskas[g], Relu Giuca[d], Anis Guelmami[e], Mirco Guerrazzi[f], Samuel Hilaire[e], Marija Kataržytė[g], Ana I. Lillebø[h], Raquel Lizán[c], Bruna R.F. Oliveira[h], Vitor H. Oliveira[h], Marta Pedrón[c], Jolita Petkuvienė[g], Tudor Racoviceanu[d], Michael Ronse[e], Chiara Santinelli[f], Ana I. Sousa[h], Wouter Suykerbuyk[i], Edvinas Tiškus[g], Claudia Tropea[f], Diana Vaičiūtė[g], Silvia Valsecchi[f], Marinka van Puijenbroek[i], Mourine J. Yegon[b], Antonio Camacho[c†], Daniel von Schiller[a†]

[a] Departament de Biologia Evolutiva, Ecologia i Ciències Ambientals, Universitat de Barcelona, Av. Diagonal 643, 08028, Barcelona, Spain
[b] WasserCluster Lunz - Biologische Station, Dr. Carl Kupelwieser Promenade 5, 3293, Lunz am See, Austria
[c] Institut Cavanilles de Biodiversitat i Biologia Evolutiva, Universitat de València, C/Catedràtic José Beltran 2, 46980, Paterna, Spain
[d] Department of Systems Ecology and Sustainability, University of Bucharest, spl. Independentei 91 - 95, 50095, Bucharest, Romania
[e] Institut de recherche pour la conservation des zones humides méditerranéennes, Tour du Valat, Le Sambuc, 13200, Arles, France
[f] Istituto di Biofisica, Consiglio Nazionale delle Ricerche (CNR) Pisa, Via Giuseppe Moruzzi 1, 56124, Pisa, Italy
[g] Marine Research Institute, Klaipėda University, Universiteto ave. 17, 92294, Klaipėda, Lithuania
[h] ECOMARE, CESAM - Centre for Environmental and Marine Studies, Department of Biology, University of Aveiro, Campus de Santiago, 3810-193, Aveiro, Portugal
[I] Wageningen Marine Research, Wageningen University & Research, Korringaweg 7, 4401 NT, Yerseke, The Netherlands

[†]These authors share last authorship as research heads
*Corresponding author, email: miguelcabrera@ub.edu

1. Supplementary methods

1.1. Detailed description of European case pilot wetlands

South-West Dutch Delta (DU)

Preserved sites consisted of Intertidal salt marshes showing natural hydrological and sedimentation processes, vegetated surfaces, and minimal disruption by coastal infrastructure. These sites maintained natural marsh integrity and ecological processes including tidal inundation patterns, natural sedimentation, pioneer zone species, and mid-upper marsh communities. The main alterations were the installation of stone breakwaters or wooden pales perpendicular to the marsh to reduce hydrodynamics and locally reduce erosion. These hard structures disrupted natural sedimentation processes and reflected wave energy, leading to accelerated lateral erosion and creek widening, prevention of natural landward marsh development and disappearance of pioneer-zone plant species. Restoration involved morphological reconstruction and recovery of natural hydrodynamics through managed realignment. In both cases, the displacement of the coastal defense line further inland facilitated recovery of natural hydrodynamics, tidal patterns, sedimentation processes, and vegetation establishment on previously reclaimed land.

Ria de Aveiro (RI)

Preserved sites exhibited healthy intertidal seagrass meadows with high coverage of *Zostera noltii,* stable sediment structure, and absence of significant anthropogenic pressures. The main alteration consisted of erosion and bioturbation from bait-digging activities and physical disturbance from trampling. Altered sites consist of bare, unvegetated intertidal areas where meadows have been lost or severely degraded. These areas exhibit high erosion, unstable sediments prone to resuspension and reduced biodiversity. Restoration actions consisted of re-vegetation: Active mosaic-pattern transplantation of *Z. noltii* have been formerly performed in zones where pressures are no longer relevant. Transplants were able to cover previously unvegetated areas and develop uniform, robust coverage throughout the restored sites within one year.

Camargue (CA)

Preserved sites were selected from mediterranean freshwater marshes and ponds that retained natural hydrological regimes and ecological features, without significant historical land use conversion or hydrological alterations. These sites maintained intact soil and seasonal flooding and drying patterns characteristic of Mediterranean freshwater wetlands, supporting native flora and fauna. This case pilot suffered mainly from hydrological, trophic, and land-use change impacts. The altered sites included former fishponds and areas that had been subjected to decades of artificial hydrological regimes, mainly favoring hunting activities. These sites experienced hydrological alterations driven by artificial irrigation and drainage systems, leading to long-term changes in water regimes. The natural seasonal hydrological variability was replaced by highly managed water regimes, with continuous flooding during dry seasons. Restoration activities involved soil, hydrology, vegetation and morphological reconstruction of former rice fields and pastures. Topographic reshaping, removal of drainage and irrigation infrastructure, soil and seed transfers allowed for the recovery of natural flooding and drying cycles, recolonization by native wetland vegetation and increasing presence of amphibians and waterbirds in the sites.

Valencian wetland Marjal dels Moros (VA)

The selected preserved sites were coastal brackish marshes with intact emergent swamp communities, natural hydrological connectivity, and limited structural and water quality degradation. These areas featured native plant communities adapted to brackish conditions (reeds, bulrush stands and halophytic shrubs) and natural hydrodynamics controlled by precipitation, evaporation and seawater intrusion via groundwater. This wetland suffers mostly from hydrological, trophic, and morphological alterations. The representative altered sites are subject to artificial water supply from irrigation and wastewater sources as well as morphological modification (land-use change and soil degradation). These pressures resulted in areas with reduced native vegetation and proliferation of invasive species, and degraded water quality with elevated nutrients and loss of characteristic brackish conditions due to desalinization. As restored sites, areas were selected where various actions were performed. Active restoration included soil reconstruction to improve substrate conditions, morphological reconstruction of natural topology and hydrological connectivity, and planting of native vegetation. Hydrological actions ensure diverse good-quality water sources to maintain aquatic refuges for fauna via flood regulation while maintaining characteristic brackish conditions. Mowing of helophytic vegetation is regularly implemented to maintain habitat heterogeneity.

Danube Delta (DA)

Preserved sites consisted of freshwater shallow lakes with native submerged (*Potamogeton spp.*, *Ceratophyllum spp.*) and floating vegetation (*Trapa natans* L., *Nymphaea alba* L.) surrounded by reed beds (*Phragmites australis* L.). These sites lacked major anthropogenic pressures, maintained their connectivity to the river network and are classified as having good ecological status according to the Water Framework Directive. The most relevant impacts of this pilot are hydrological and morphological alterations related to land-use change. Altered sites were former freshwater wetlands converted to dryland during the 1980s. One site consisted of an agricultural field used to grow cereal. The other site was initially used for pasture for cattle but was flooded due to dike failure and was subsequently abandoned for this use. These areas suffered lack of native vegetation, soil alteration and high nutrient loads from fertilizers and manure, respectively. Restoration activities consisted of the morphological and hydrological reconstruction of wetland habitats from former pastures and degraded wetlands. Restoration of sites involved the recovery of natural hydrological regimes via their re-connection to the river network and flood management via pumping stations, as well as the removal of excess reed cover to create open water habitats.

Curonian Lagoon (CU)

Preserved sites consisted of littoral zones characterized by high coverage of submerged aquatic vegetation (*Chara contraria, Chara apsera, Chara globularis, Potamogeton perfoliatus, Stuckenia pectinata*), with sandy or mixed bottom substrates and emergent reeds (*P. Australis*). The relatively low nutrient loads and chlorophyll-a concentrations of these areas are characteristic of balanced trophic conditions in the Lagoon. The most relevant pressures within the system consist of eutrophication and organic matter enrichment. Altered trophic state is driven by high nutrient loads from agricultural runoff and insufficient wastewater treatment from the Neumas river. The altered sites selected were characterized by elevated nutrient levels and associated high chlorophyll-a concentrations with episodic cyanobacterial blooms. The accumulation of organic-rich mud in the substrate promotes anoxic conditions and leads to a reduction in submerged aquatic vegetation. Restoration actions at the watershed level aimed at improving water quality and local-scale measures, such as reed harvesting to reduce excess nutrients and organic matter. Improvements of wastewater treatment infrastructure and reduced fertilizer use

in the upstream Nemunas river basin led to reduced nutrient loads. In addition, hydrological changes such as increased brackish water intrusions due to the artificial deepening of the Klaipėda Strait channel (Stakėnienė et al., 2023) and decreased annual runoff from the Nemunas River (Idzelyte- et al., 2023) have likely reduced fine sediment inputs and muddy sediment accumulation. These changes have affected recovery of sandy sediment areas and promoted the expansion of submerged aquatic vegetation in restored sites.

1.2. Best-flux estimate selection

A common set of sequential criteria was followed to select a best-flux estimate from those produced by the three models: two-point, linear model (LM) and a non-linear (HM) (Hutchinson & Mosier, 1981) regression model. Choosing an appropriate flux calculation method is not trivial, as different approaches can result in large differences in estimated flux and have different sensitivities to non-linear patterns of gas concentration within the chamber, which may arise from both instrument noise and natural processes. On the one hand, simple linear regression (LM) often underestimates fluxes in non-steady chambers (Silva et al., 2015), which leads many researchers to default to non-linear (HM) model (Rheault et al., 2024). However, noisy measurements can lead to the HM model producing unrealistic fluxes (Hüppi et al., 2018). Additionally, ebullitive dynamics typically force extreme curvatures of HM and might even cause negative LM flux estimates. To select an appropriate best-estimate instantaneous flux for every time series, we used sequential criteria based on the presence of ebullitive patterns and on LM and HM model fit statistics. This set of criteria was designed to balance the model-specific risks of over- and underestimation of fluxes, especially for cases with ebullitive patterns, while preserving a transparent and reproduceable approach.

First, all CH_4 timeseries with visual evidence of ebullition (recorded during previous inspection) were assigned to the two-point flux estimate unless the linear model presented an R^2 above 0.99 (LM.r2 > 0.99). For the rest of the timeseries, absent of ebullitive patterns, the HM model was chosen only when all the following criteria were met (defaulting to the LM estimate when one or more were violated): HM model produces a valid flux estimate (HM.flux ≠ NA); LM flux estimate is above the minimal detectable flux (Christiansen et al., 2015); HM curvature parameter *Kappa* is below the theoretical maximum (Hüppi et al., 2018); The ratio between the non-linear (HM) flux estimate and the linear (LM) estimate, the g-fact (Hüppi et al., 2018) is below the gas species-specific custom threshold (CO_2 g-fact < 4; CH_4 g-fact < 3); Akaike Information Criterion corrected for small sample size (AICc) of the HM model is lower than that of the LM model; Mean absolute error (MAE) of HM model is at least 5% lower than that of LM model.

A larger g-fact threshold was allowed for CO_2 time series (compared to CH_4) to account for cases where CO_2 concentration inside the chamber might cause limitation of photosynthetic activity and associated attenuation of uptake rate during the incubation. Using this set of criteria, the chosen best model for CO_2 fluxes was LM for 1914 timeseries (64%) and HM for 1076 timeseries (36%). For CH_4 fluxes, the best model was two-point for 631 (21.1%), LM for 1850 (62%) and HM for 505 (16.9%) of the time series.

2. Supplementary Figures

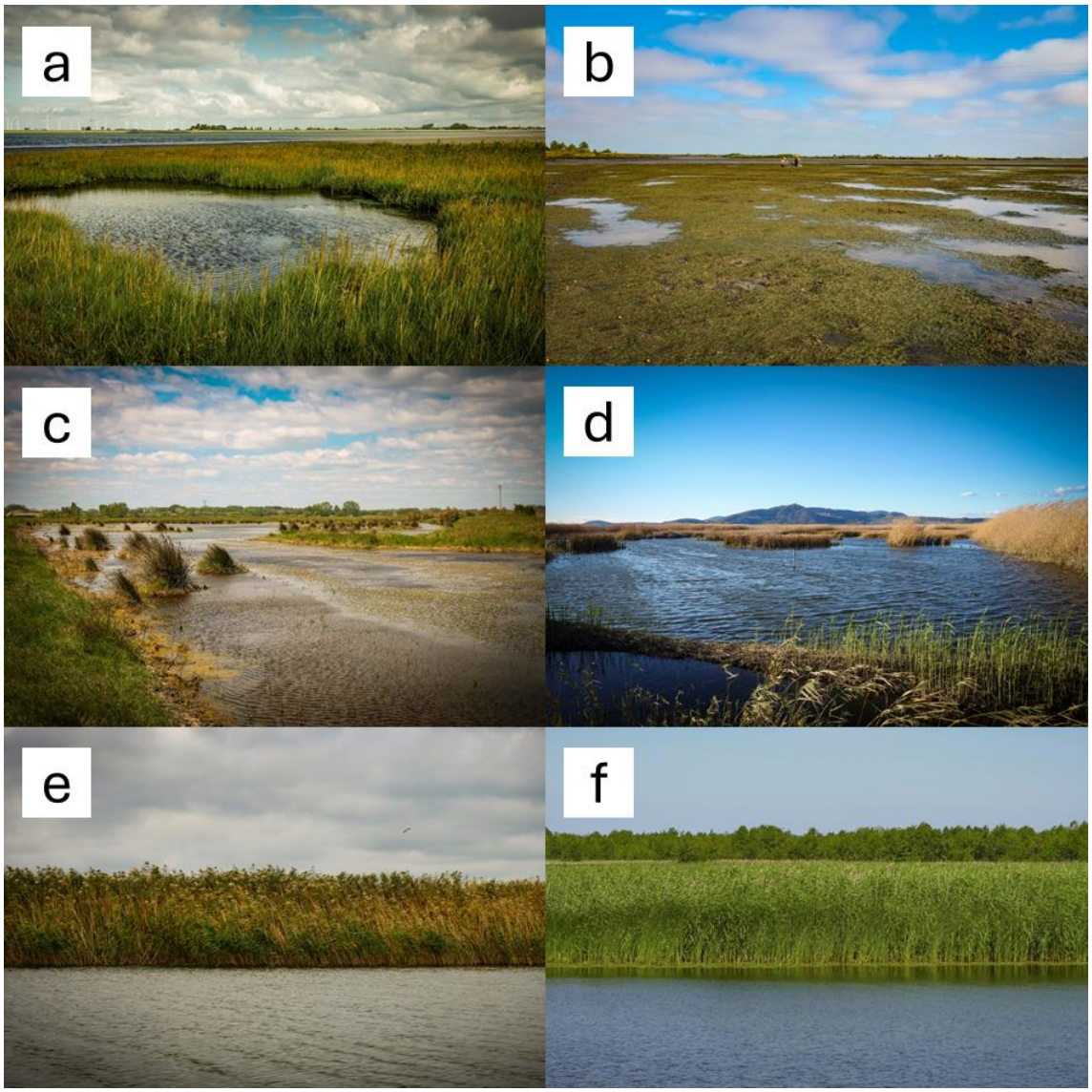

Figure S1. Representative pictures of case pilot preserved wetlands. Pictures depict (a) saltmarsh of South-west Dutch Delta (DU), (b) Zostera noltii meadow during low tide in Ria de Aveiro (RI), (c) freshwater marshes and ponds of Camargue (CA), (d) brackish marshes of Marjal dels Moros (VA), (e) freshwater lakes with reed beds of Danube Delta (DA), (f) freshwater littoral with reeds and submerged vegetation of Curonian Lagoon (CU). Pictures facilitated by LifeWatch ERIC.

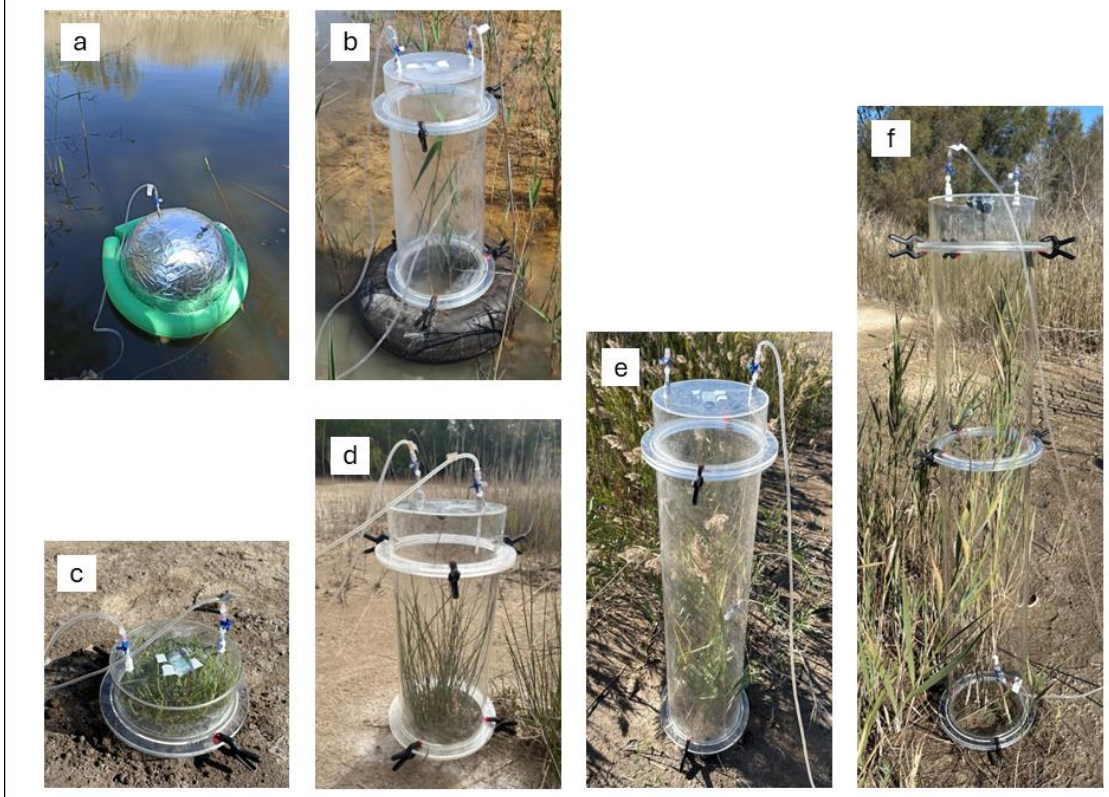

Figure S2. Static chamber types and configurations. (a) Opaque semi-spherical floating chamber used in open water areas, (b) transparent modular cylindrical chamber with floating device used in flooded areas with emergent vegetation, (c-f) transparent modular cylindrical chamber used in non-flooded areas in increasing-volume configurations. Dark incubations using the cylindrical modular chamber involved the use of an opaque textile cover (not shown).

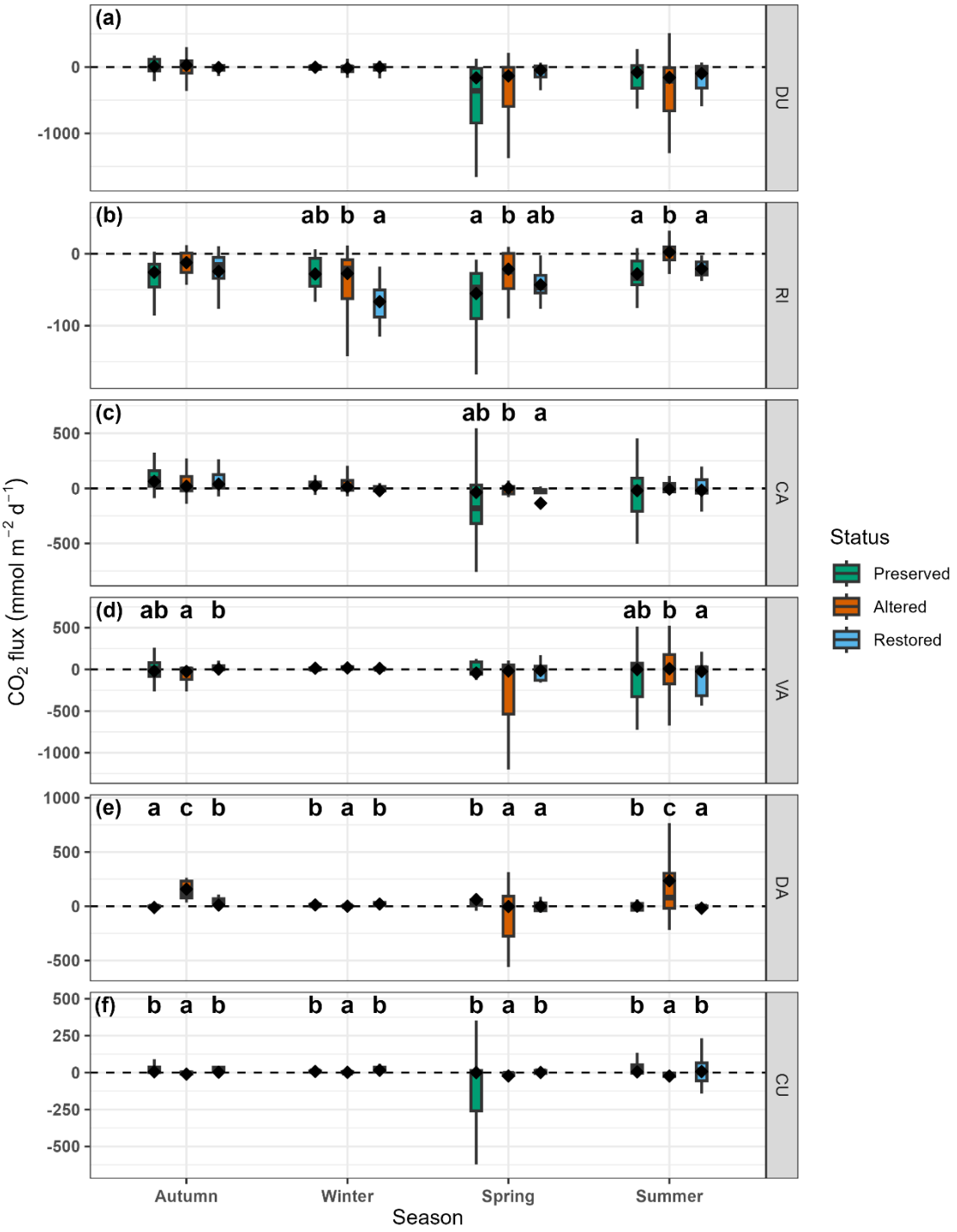

Figure S3. CO_2 fluxes (mmol m^{-2} d^{-1}) across seasons according to wetland conservation status for each case pilot (a-f panels). Boxplots show the median, interquartile range, and whiskers extending to 1.5×IQR; data outside these ranges are not displayed for clarity. Diamonds represent estimated marginal means (EMMs) derived from parametric bootstrap distributions (5000 iterations). Different letters indicate significant differences among EMMs within each season based on Holm-adjusted empirical pairwise contrasts ($p < 0.05$).

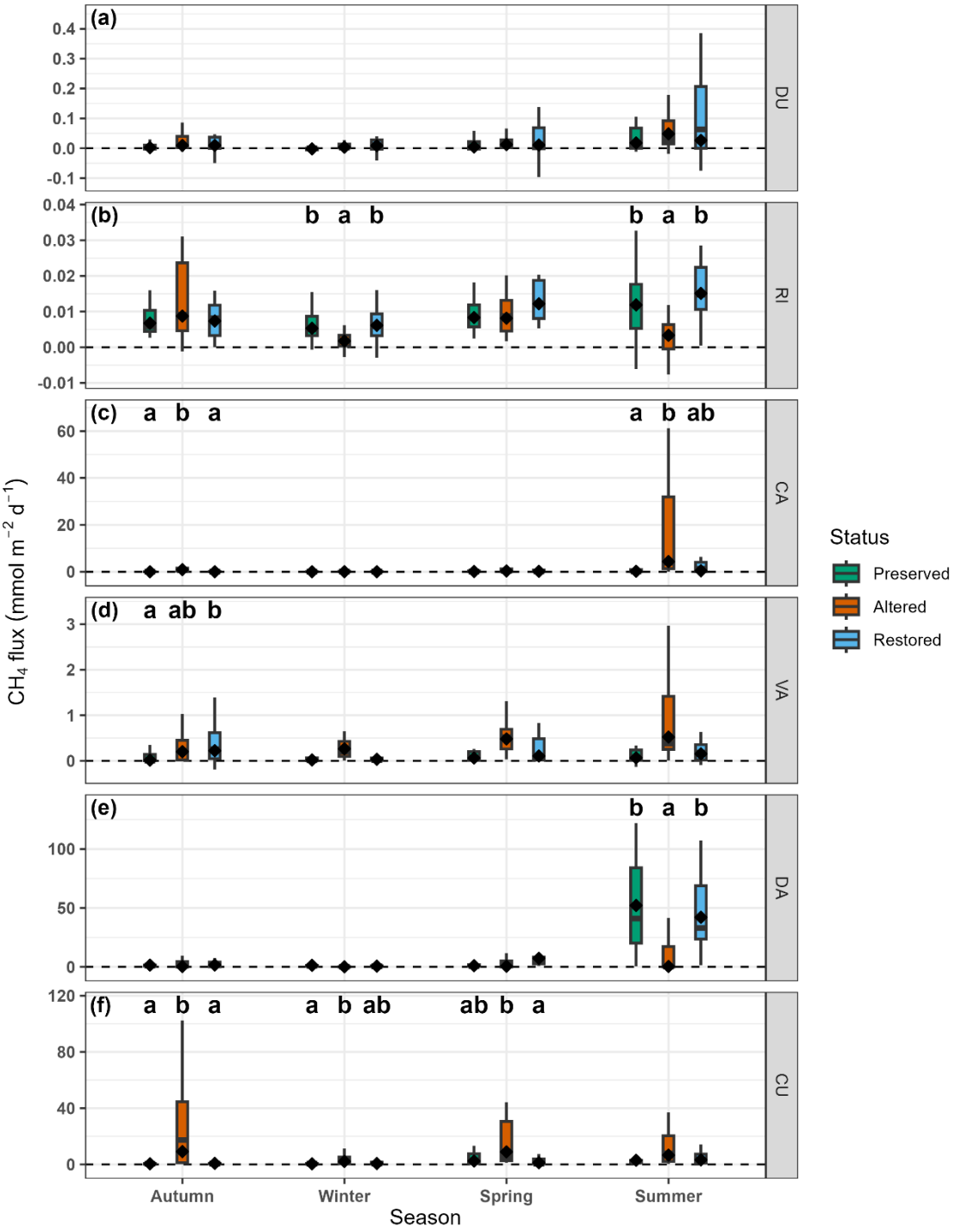

Figure S4. CH_4 fluxes (mmol m^{-2} d^{-1}) across seasons according to wetland conservation status for each case pilot (a-f panels). Boxplots show the median, interquartile range, and whiskers extending to 1.5×IQR; data outside these ranges are not displayed for clarity. Diamonds represent estimated marginal means (EMMs) derived from parametric bootstrap distributions (5000 iterations). Different letters indicate significant differences among EMMs within each season based on Holm-adjusted empirical pairwise contrasts ($p < 0.05$).

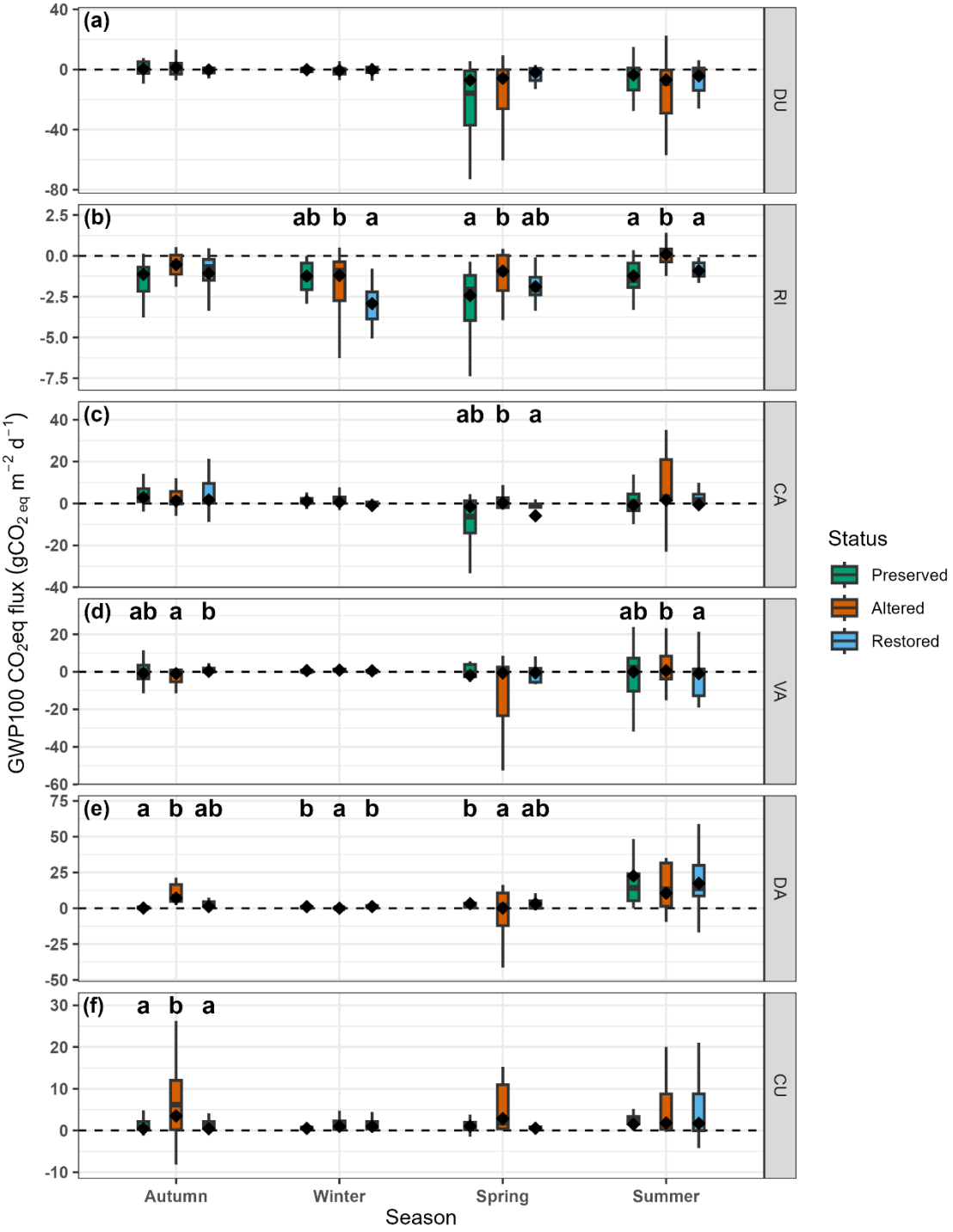

Figure S5a. GWP100 CO_2-eq fluxes (g CO_2-eq m^{-2} d^{-1}) across seasons according to wetland conservation status for each case pilot (a-f panels). Boxplots show the median, interquartile range, and whiskers extending to 1.5×IQR; data outside these ranges are not displayed for clarity. Diamonds represent estimated marginal means (EMMs) derived from paired parametric bootstrap distributions of CO_2 and CH_4 models (5000 iterations). Different letters indicate significant differences among EMMs within each season based on Holm-adjusted empirical pairwise contrasts ($p < 0.05$).

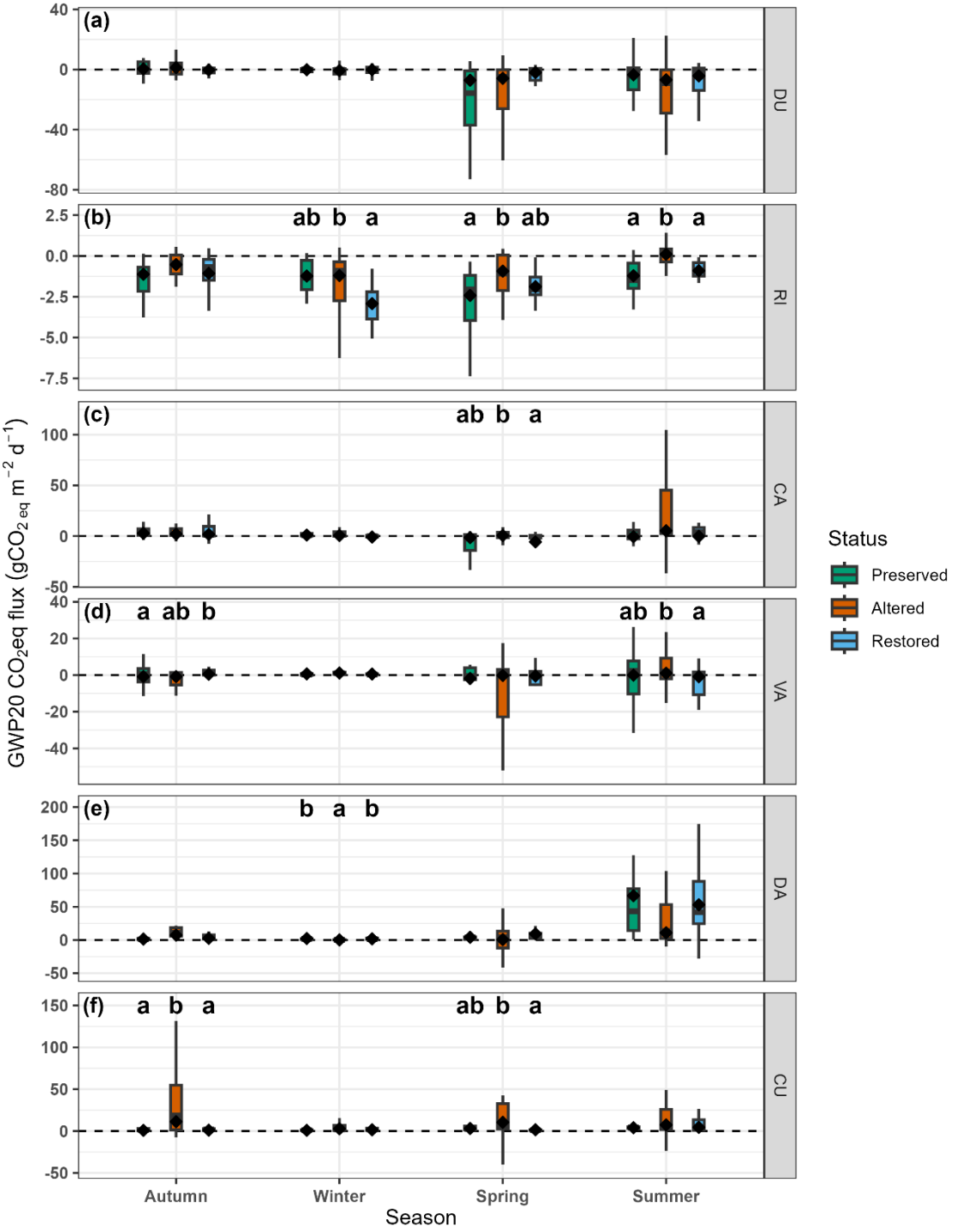

Figure S5b. GWP20 CO_2-eq fluxes (g CO_2-eq m^{-2} d^{-1}) across seasons according to wetland conservation status for each case pilot (a-f panels). Boxplots show the median, interquartile range, and whiskers extending to 1.5×IQR; data outside these ranges are not displayed for clarity. Diamonds represent estimated marginal means (EMMs) derived from paired parametric bootstrap distributions of CO_2 and CH_4 models (5000 iterations). Different letters indicate significant differences among EMMs within each season based on Holm-adjusted empirical pairwise contrasts ($p < 0.05$).

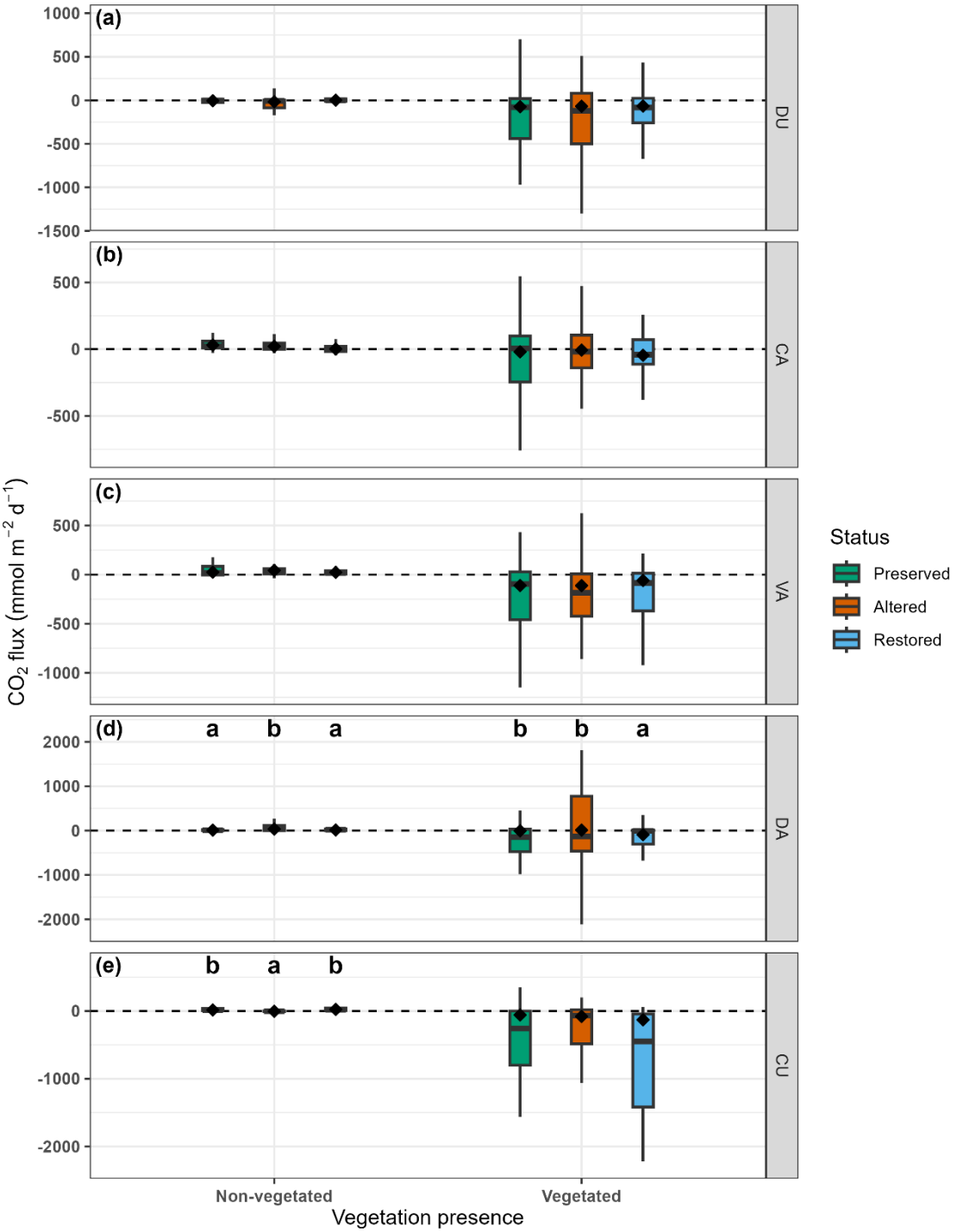

Figure S6. CO_2 fluxes (mmol m^{-2} d^{-1}) according to vegetation presence and wetland conservation status for each case pilot (a-f panels). Boxplots show the median, interquartile range, and whiskers extending to 1.5×IQR; data outside these ranges are not displayed for clarity. Diamonds represent estimated marginal means (EMMs) derived from parametric bootstrap distributions (5000 iterations). Different letters indicate significant differences among EMMs within vegetation presence category based on Holm-adjusted empirical pairwise contrasts ($p < 0.05$).

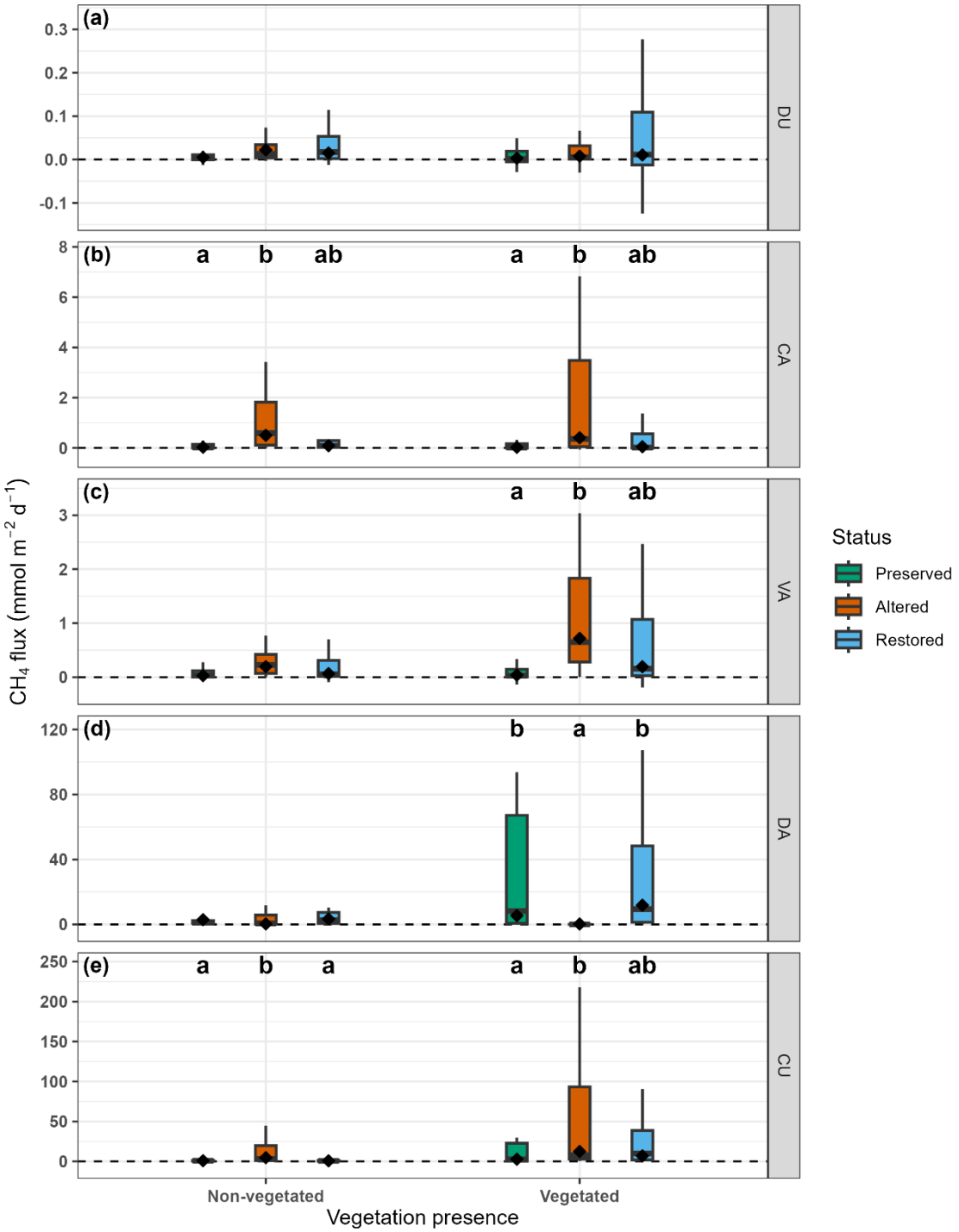

Figure S7. CH_4 fluxes (mmol m^{-2} d^{-1}) according to vegetation presence and wetland conservation status for each case pilot (a-f panels). Boxplots show the median, interquartile range, and whiskers extending to 1.5×IQR; data outside these ranges are not displayed for clarity. Diamonds represent estimated marginal means (EMMs) derived from parametric bootstrap distributions (5000 iterations). Different letters indicate significant differences among EMMs within vegetation presence category based on Holm-adjusted empirical pairwise contrasts ($p < 0.05$).

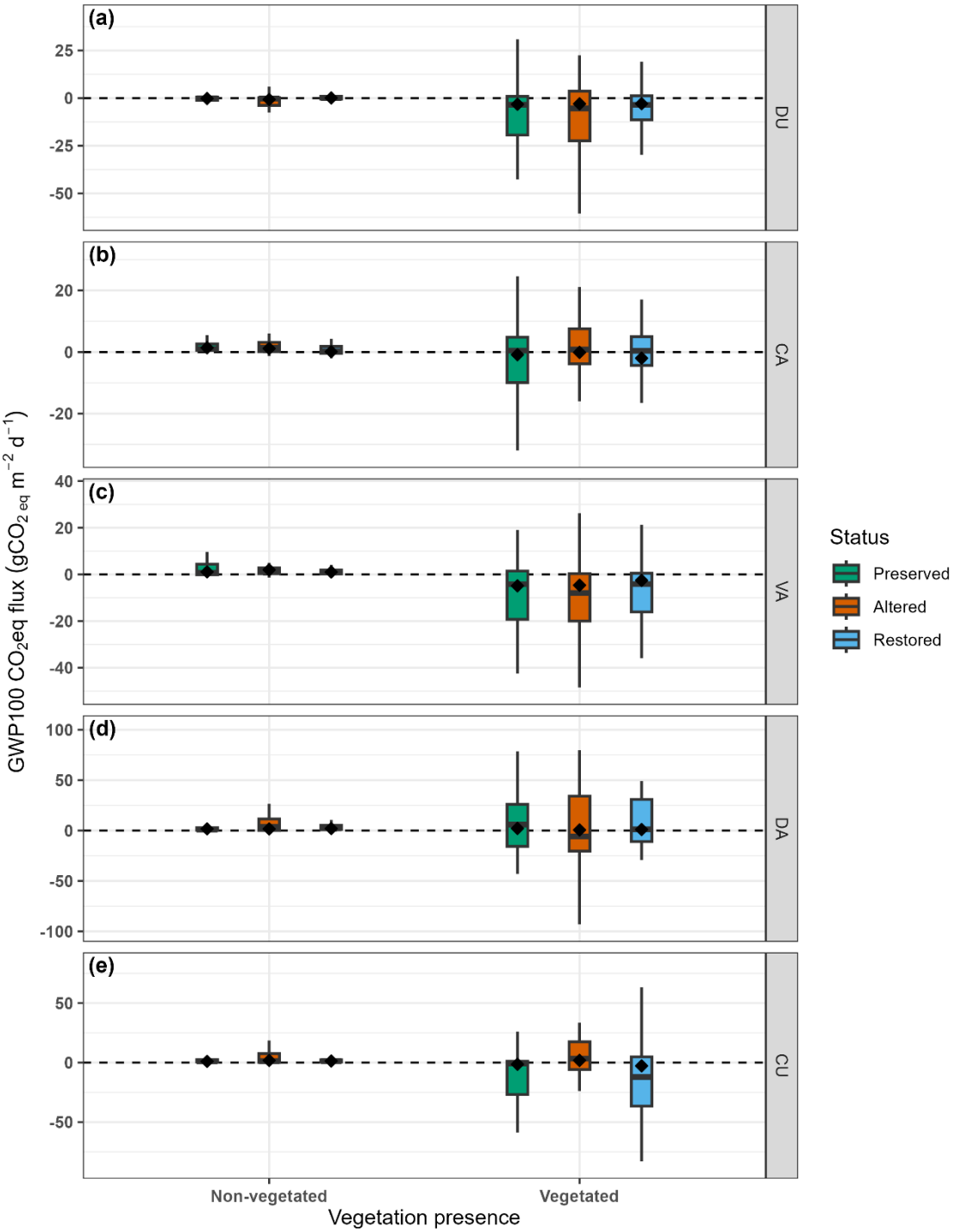

Figure S8a. GWP100 CO_2-eq fluxes (g CO_2-eq m^{-2} d^{-1}) according to vegetation presence and wetland conservation status for each case pilot (a-f panels). Boxplots show the median, interquartile range, and whiskers extending to 1.5×IQR; data outside these ranges are not displayed for clarity. Diamonds represent estimated marginal means (EMMs) derived from paired parametric bootstrap distributions of CO_2 and CH_4 models (5000 iterations). No significant pairwise contrasts were detected within vegetation presence categories after Holm correction ($p \geq 0.05$).

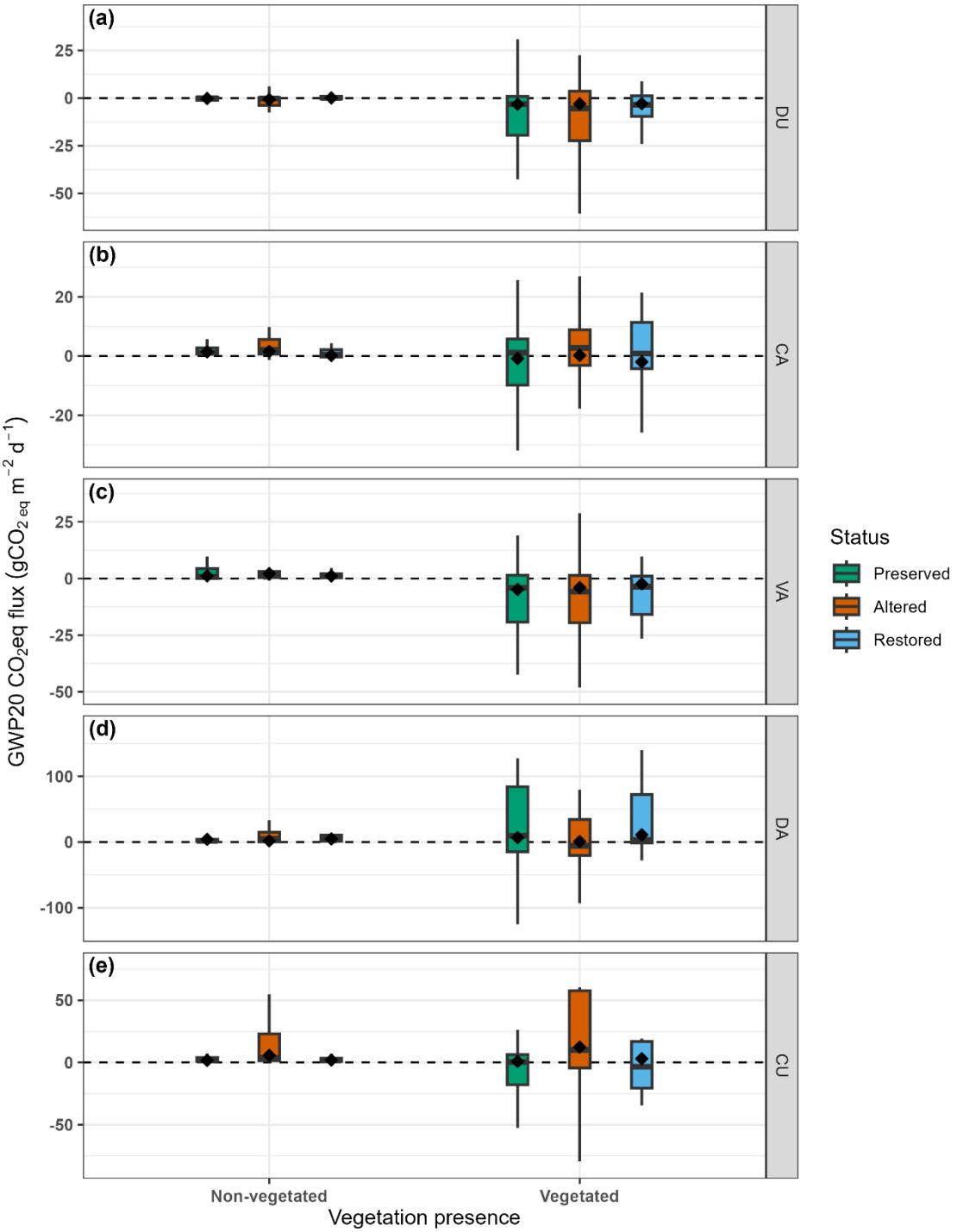

Figure S8b. GWP20 CO_2-eq fluxes (g CO_2-eq m^{-2} d^{-1}) according to vegetation presence and wetland conservation status for each case pilot (a-f panels). Boxplots show the median, interquartile range, and whiskers extending to 1.5×IQR; data outside these ranges are not displayed for clarity. Diamonds represent estimated marginal means (EMMs) derived from paired parametric bootstrap distributions of CO_2 and CH_4 models (5000 iterations). No significant pairwise contrasts were detected within vegetation presence categories after Holm correction ($p \geq 0.05$).

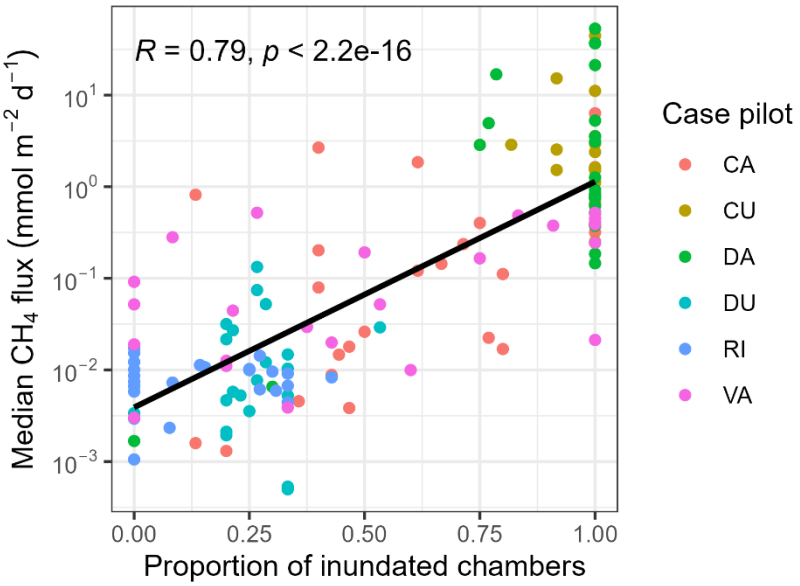

Figure S9. Cross system relationship between proportion of chambers deployed in inundated areas during each site sampling event and median CH_4 flux. Each point represents one seasonal visit to one site of one case pilot. Solid line is the linear regression across all observations, with the corresponding Pearson correlation coefficient (R) and p-value. CH_4 flux is displayed on a logarithmic scale.

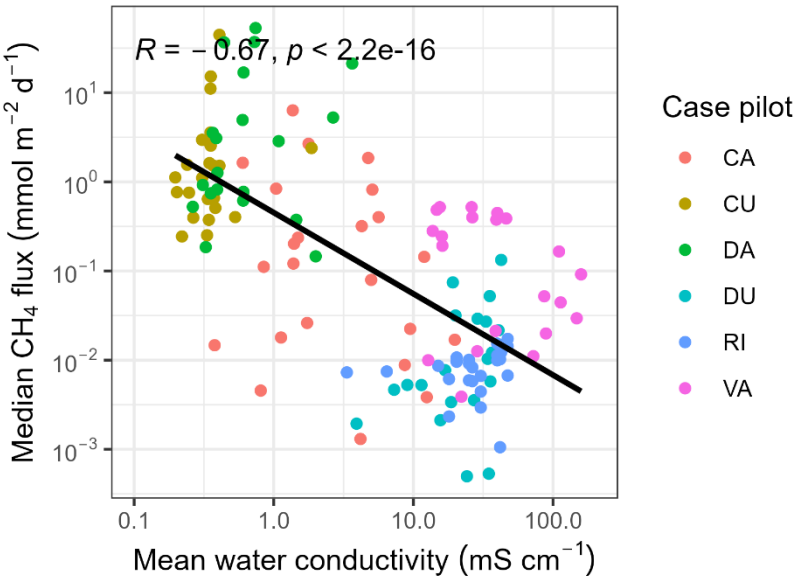

Figure S10. Cross system relationship between sampling-level mean water conductivity and median CH_4 flux. Each point represents one seasonal visit to one site of one case pilot. Solid line is the linear regression across all observations, with the corresponding Pearson correlation coefficient (R) and p-value. Both conductivity and CH_4 flux are displayed on logarithmic scales.

3. Supplementary tables

Table S1. GLMM model summaries for CO_2 and CH_4. Model structure (formula call, distribution and data transformation), number of samples (N), marginal and conditional R-squared values (R^2m and R^2c) representing the proportion of variance explained by the model, and significance (p-value) of fixed effects (conservation status, season, vegetation presence and interactions) for each case pilot-GHG dataset.

Dataset	Best-Supported Model	N	R^2m	R^2c	Effect	p-value
DU - CO_2	Call: Flux ~ status * season * vegpresence + (1 | subsite), Distribution: t, Transformation: pseudo-log	349	0.493	0.514	status	0.771
					season	< 0.001
					vegpresence	< 0.001
					status : season	0.011
					status : vegpresence	0.403
					status : season : vegpresence	0.014
RI - CO_2	Call: Flux ~ status * season + (1 | subsite), Distribution: gaussian, Transformation: pseudo-log	266	0.313	0.345	status	< 0.001
					season	< 0.001
					status : season	0.001
CA - CO_2	Call: Flux ~ status * season * vegpresence + (1 | subsite), Distribution: t, Transformation: pseudo-log	346	0.471	0.534	status	0.27
					season	< 0.001
					vegpresence	< 0.001
					status : season	< 0.001
					status : vegpresence	0.214
					status : season : vegpresence	< 0.001

Dataset	Best-Supported Model	N	R^2m	R^2c	Effect	p-value
VA - CO_2	Call: Flux ~ status * season * vegpresence + (1 | subsite), Distribution: t, Transformation: pseudo-log	340	0.741	0.750	status	0.631
					season	< 0.001
					vegpresence	< 0.001
					status : season	< 0.001
					status : vegpresence	0.002
					status : season : vegpresence	< 0.001
DA - CO_2	Call: Flux ~ status * season * vegpresence + (1 | subsite), Distribution: t, Transformation: pseudo-log	296	0.780	0.783	status	< 0.001
					season	< 0.001
					vegpresence	< 0.001
					status : season	< 0.001
					status : vegpresence	< 0.001
					status : season : vegpresence	< 0.001
CU - CO_2	Call: Flux ~ status * season * vegpresence + (1 | subsite), Distribution: t, Transformation: pseudo-log	320	0.760	0.761	status	< 0.001
					season	< 0.001
					vegpresence	< 0.001
					status : season	< 0.001
					status : vegpresence	< 0.001
					status : season : vegpresence	< 0.001

Dataset	Best-Supported Model	N	R^2m	R^2c	Effect	p-value
DU - CH_4	Call: Flux ~ status * season * vegpresence + (1 | subsite), Distribution: gaussian, Transformation: pseudo-log	346	0.139	0.284	status	0.523
					season	< 0.001
					vegpresence	0.022
					status : season	0.726
					status : vegpresence	0.414
					status : season : vegpresence	0.93
RI - CH_4	Call: Flux ~ status * season + (1 | subsite), Distribution: t, Transformation: pseudo-log	265	0.225	0.229	status	< 0.001
					season	< 0.001
					status : season	< 0.001
CA - CH_4	Call: Flux ~ status * season * vegpresence + (1 | subsite), Distribution: gaussian, Transformation: pseudo-log	345	0.390	0.436	status	0.001
					season	< 0.001
					vegpresence	0.222
					status : season	< 0.001
					status : vegpresence	0.782
					status : season : vegpresence	0.485
VA - CH_4	Call: Flux ~ status * season * vegpresence + (1 | subsite), Distribution: t, Transformation: pseudo-log	337	0.311	0.450	status	0.022
					season	< 0.001
					vegpresence	< 0.001
					status : season	0.004
					status : vegpresence	0.055
					status : season : vegpresence	0.511

Dataset	Best-Supported Model	N	R^2m	R^2c	Effect	p-value
DA - CH_4	Call: Flux ~ status * season * vegpresence + (1 | subsite), Distribution: t, Transformation: log	306	0.503	0.678	status	0.011
					season	< 0.001
					vegpresence	0.025
					status : season	< 0.001
					status : vegpresence	0.046
					status : season : vegpresence	< 0.001
CU - CH_4	Call: Flux ~ status * season * vegpresence + (1 | subsite), Distribution: gaussian, Transformation: pseudo-log	317	0.522	0.581	status	0.003
					season	< 0.001
					vegpresence	< 0.001
					status : season	< 0.001
					status : vegpresence	0.01
					status : season : vegpresence	0.006

Table S2. Bootstrap-derived estimated marginal means (EMMs) of GHG fluxes. EMMs, standard errors (SE) and 95% confidence intervals (95% CI) of GHG fluxes (CO_2, CH_4, GWP100 CO_2-eq, GWP20 CO_2-eq) for the different conservation statuses of each case pilot wetland across seasons and vegetation presence. Estimates and uncertainty metrics were derived from paired parametric bootstrap distributions (5000 iterations; see Methods), with CO_2-eq values calculated after application of the corresponding CH_4 GWP scaling factors.

Case pilot	Status	CO2 flux (mol m^{-2} y^{-1})		CH4 flux (mmol m^{-2} y^{-1})		GWP100 flux (g CO2eq. m^{-2} y^{-1})		GWP20 flux (g CO2eq. m^{-2} y^{-1})	
		Mean ± SE	95% CI	Mean ± SE	95% CI	Mean ± SE	95% CI	Mean ± SE	95% CI
RI	Preserved	-11.95 ± 1.93	-16.09 to -8.51	2.827 ± 0.275	2.314 to 3.399	-524.6 ± 84.9	-706.9 to -373.1	-522.2 ± 84.9	-704.4 to -370.6
	Altered	-4.97 ± 1.29	-7.69 to -2.61	1.820 ± 0.200	1.443 to 2.237	-218.1 ± 56.9	-337.5 to -114.0	-216.6 ± 56.9	-335.9 to -112.8
	Restored	-13.01 ± 2.08	-17.34 to -9.23	3.496 ± 0.357	2.840 to 4.238	-570.9 ± 91.5	-761.2 to -404.9	-567.9 ± 91.5	-758.2 to -402.0
DU	Preserved	-13.49 ± 4.71	-23.68 to -5.33	1.31 ± 1.59	-0.91 to 5.22	-593 ± 207	-1042 to -235	-592 ± 207	-1040 to -234
	Altered	-15.32 ± 5.05	-26.56 to -6.69	4.38 ± 4.01	0.36 to 13.99	-672 ± 222	-1167 to -292	-669 ± 222	-1164 to -288
	Restored	-11.16 ± 4.43	-20.60 to -3.31	4.34 ± 3.67	0.39 to 14.03	-489 ± 195	-905 to -144	-485 ± 195	-902 to -141
CA	Preserved	1.46 ± 4.05	-6.13 to 10.09	9.57 ± 5.97	2.48 to 24.55	69 ± 178	-265 to 448	77 ± 178	-258 to 454
	Altered	2.30 ± 4.09	-5.34 to 10.73	160.5 ± 94.5	46.3 to 410.4	171 ± 185	-177 to 565	306 ± 219	-81 to 786
	Restored	-6.61 ± 4.80	-17.57 to 1.61	23.4 ± 14.1	6.5 to 60.1	-281 ± 212	-766 to 82	-261 ± 212	-746 to 103
VA	Preserved	-3.73 ± 1.66	-7.17 to -0.61	11.37 ± 7.96	2.30 to 31.93	-159.1 ± 73.3	-310.9 to -21.1	-149.5 ± 73.9	-302.9 to -9.5
	Altered	-1.36 ± 1.59	-4.58 to 1.64	119.8 ± 83.3	29.6 to 340.6	-8.1 ± 78.5	-164.9 to 148.4	93 ± 127	-106 to 392
	Restored	-1.72 ± 1.64	-5.19 to 1.26	36.9 ± 24.7	9.1 to 102.4	-59.8 ± 72.6	-212.3 to 73.3	-28.7 ± 78.1	-188.8 to 122.2
DA	Preserved	2.448 ± 0.629	1.304 to 3.793	1177 ± 1040	182 to 4054	617 ± 450	179 to 1868	1612 ± 1330	336 to 5319
	Altered	9.95 ± 1.67	6.68 to 13.48	100 ± 103	5 to 365	481.1 ± 85.7	328.1 to 669.5	566 ± 151	361 to 935
	Restored	0.893 ± 0.500	-0.078 to 1.907	1534 ± 1310	262 to 5005	704 ± 568	151 to 2196	2000 ± 1680	377 to 6428
CU	Preserved	1.388 ± 0.300	0.830 to 2.017	378 ± 137	180 to 712	224.7 ± 61.0	135.1 to 372.3	544 ± 176	290 to 974
	Altered	-3.391 ± 0.526	-4.510 to -2.449	2069 ± 722	994 to 3814	747 ± 313	278 to 1518	2496 ± 922	1116 to 4751
	Restored	1.704 ± 0.340	1.084 to 2.426	408 ± 144	193 to 749	251.7 ± 63.9	153.9 to 401.9	597 ± 185	321 to 1034

Table S3. Post-hoc contrasts between conservation-status EMMs of GHG fluxes. Post-hoc contrasts between estimated marginal means (EMMs) of (a) CO_2, (b) CH_4, (c) GWP100 CO_2-eq, and (d) GWP20 CO_2-eq fluxes among conservation status classes for each case pilot across seasons and vegetation presence. Estimates, standard errors (SE), 95% confidence intervals (95% CI), and empirical p-values are derived from parametric bootstrap distributions (5000 iterations; see Methods). CO_2-eq contrasts were calculated from paired CO_2 and CH_4 bootstrap distributions after application of the corresponding CH_4 GWP scaling factors. Negative Preserved–Altered contrasts represent avoided emissions through conservation. Negative Restored–Altered contrasts represent mitigated emissions through restoration. Positive Restored–Preserved contrasts represent functional recovery debt associated with restoration.

Table S3a. CO_2 flux contrasts.

Case pilot	Contrast	Difference (mol CO_2 m^{-2} y^{-1})		
		Estimate ± SE	95% CI	p-value
DU	Preserved - Altered	1.84 ± 6.85	-11.20 to 15.83	1
	Restored - Altered	4.16 ± 6.71	-8.71 to 17.68	1
	Restored - Preserved	2.33 ± 6.40	-10.29 to 14.85	1
RI	Preserved - Altered	-6.97 ± 2.31	-11.73 to -2.61	0.002
	Restored - Altered	-8.03 ± 2.45	-12.88 to -3.30	< 0.001
	Restored - Preserved	-1.06 ± 2.86	-6.75 to 4.52	0.711
CA	Preserved - Altered	-0.84 ± 5.70	-12.26 to 10.16	0.89
	Restored - Altered	-8.91 ± 6.39	-22.20 to 2.58	0.398
	Restored - Preserved	-8.07 ± 6.26	-21.51 to 3.51	0.398
VA	Preserved - Altered	-2.36 ± 2.28	-6.86 to 1.96	0.929
	Restored - Altered	-0.36 ± 2.29	-4.89 to 4.17	0.929
	Restored - Preserved	2.00 ± 2.35	-2.55 to 6.60	0.929
DA	Preserved - Altered	-7.50 ± 1.78	-11.12 to -4.04	< 0.001
	Restored - Altered	-9.05 ± 1.74	-12.66 to -5.72	< 0.001
	Restored - Preserved	-1.555 ± 0.798	-3.141 to -0.074	0.042
CU	Preserved - Altered	4.779 ± 0.605	3.716 to 6.035	< 0.001
	Restored - Altered	5.096 ± 0.624	3.947 to 6.424	< 0.001
	Restored - Preserved	0.316 ± 0.457	-0.583 to 1.224	0.495

Table S3b. CH_4 flux contrasts.

Case pilot	Contrast	Difference (mmol CH_4 m^{-2} y^{-1})		
		Estimate ± SE	95% CI	p-value
DU	Preserved - Altered	-3.07 ± 4.32	-13.05 to 2.76	1
	Restored - Altered	-0.03 ± 5.45	-11.05 to 10.84	1
	Restored - Preserved	3.03 ± 3.99	-2.76 to 13.11	1
RI	Preserved - Altered	1.007 ± 0.337	0.345 to 1.674	0.006
	Restored - Altered	1.676 ± 0.410	0.893 to 2.492	< 0.001
	Restored - Preserved	0.669 ± 0.452	-0.218 to 1.568	0.134
CA	Preserved - Altered	-150.9 ± 94.7	-399.7 to -36.0	0.001
	Restored - Altered	-137.1 ± 95.8	-388.1 to -16.6	0.029
	Restored - Preserved	13.8 ± 15.3	-9.5 to 50.8	0.256
VA	Preserved - Altered	-108.4 ± 83.7	-326.8 to -16.2	0.022
	Restored - Altered	-82.9 ± 87.0	-303.3 to 28.7	0.347
	Restored - Preserved	25.5 ± 25.9	-9.1 to 90.7	0.347
DA	Preserved - Altered	1077 ± 1040	48 to 3928	0.066
	Restored - Altered	1434 ± 1310	136 to 4872	0.041
	Restored - Preserved	357 ± 1680	-3037 to 4025	0.79
CU	Preserved - Altered	-1691 ± 735	-3444 to -555	< 0.001
	Restored - Altered	-1661 ± 737	-3429 to -531	< 0.001
	Restored - Preserved	30 ± 202	-380 to 427	0.876

Table S3c. GWP100 CO_2-eq flux contrasts.

Case pilot	Contrast	Difference (g CO_2-eq. m^{-2} y^{-1}, GWP100)		
		Estimate ± SE	95% CI	p-value
DU	Preserved - Altered	79 ± 301	-494 to 696	1
	Restored - Altered	183 ± 295	-384 to 779	1
	Restored - Preserved	104 ± 282	-452 to 654	1
RI	Preserved - Altered	-306 ± 102	-516 to -114	0.002
	Restored - Altered	-353 ± 108	-566 to -145	< 0.001
	Restored - Preserved	-46 ± 126	-297 to 199	0.712
CA	Preserved - Altered	-102 ± 255	-611 to 399	0.687
	Restored - Altered	-452 ± 284	-1049 to 52	0.246
	Restored - Preserved	-349 ± 276	-943 to 162	0.361
VA	Preserved - Altered	-151 ± 107	-366 to 50	0.467
	Restored - Altered	-52 ± 107	-265 to 156	0.672
	Restored - Preserved	99 ± 104	-103 to 304	0.672
DA	Preserved - Altered	136 ± 455	-355 to 1389	1
	Restored - Altered	223 ± 576	-380 to 1760	1
	Restored - Preserved	86 ± 729	-1382 to 1675	1
CU	Preserved - Altered	-522 ± 319	-1281 to -27	0.091
	Restored - Altered	-495 ± 320	-1267 to -0	0.1
	Restored - Preserved	27.0 ± 89.8	-157.1 to 206.5	0.743

Table S3d. GWP20 CO_2-eq flux contrasts.

Case pilot	Contrast	Difference (g CO_2-eq. m^{-2} y^{-1}, GWP20)		
		Estimate ± SE	95% CI	p-value
DU	Preserved - Altered	77 ± 302	-496 to 692	1
	Restored - Altered	183 ± 295	-384 to 781	1
	Restored - Preserved	106 ± 282	-447 to 659	1
RI	Preserved - Altered	-306 ± 102	-515 to -113	0.002
	Restored - Altered	-351 ± 108	-565 to -144	< 0.001
	Restored - Preserved	-46 ± 126	-297 to 200	0.716
CA	Preserved - Altered	-230 ± 280	-802 to 296	0.395
	Restored - Altered	-567 ± 306	-1229 to -37	0.112
	Restored - Preserved	-338 ± 276	-928 to 175	0.395
VA	Preserved - Altered	-243 ± 146	-579 to 5	0.164
	Restored - Altered	-122 ± 149	-453 to 134	0.533
	Restored - Preserved	121 ± 108	-89 to 336	0.533
DA	Preserved - Altered	1047 ± 1330	-287 to 4715	0.553
	Restored - Altered	1435 ± 1680	-235 to 5888	0.553
	Restored - Preserved	388 ± 2150	-3942 to 5068	0.834
CU	Preserved - Altered	-1952 ± 939	-4188 to -497	0.005
	Restored - Altered	-1900 ± 942	-4176 to -447	0.006
	Restored - Preserved	53 ± 259	-471 to 568	0.821

Table S4. Summary of surface water parameters for different conservation status of each case pilot wetland. Chlorophyll-a (Chl-a), electrical conductivity (EC), total nitrogen (Total N) and total phosphorus (Total P) were determined using common analytical techniques (Santinelli et al., submitted). Total nitrogen and phosphorus include both particulate and dissolved nutrients.

Case pilot	Status	N	Chl-a (µg L^{-1})	EC (mS cm^{-1})	Total N (µM)	Total P (µM)
			Mean ± SE	Mean ± SE	Mean ± SE	Mean ± SE
DU	Preserved	24	4.40 ± 0.77	22.73 ± 2.57	90.98 ± 13.39	3.85 ± 0.49
	Altered	24	7.17 ± 2.87	24.75 ± 2.40	92.29 ± 15.65	13.01 ± 4.51
	Restored	24	3.66 ± 0.72	23.47 ± 2.64	107.24 ± 14.28	5.53 ± 0.84
RI	Preserved	24	1.66 ± 0.25	32.76 ± 2.60	40.76 ± 4.65	1.38 ± 0.06
	Altered	24	1.76 ± 0.21	26.16 ± 2.90	75.40 ± 9.28	1.62 ± 0.06
	Restored	24	3.18 ± 0.51	25.28 ± 3.31	113.47 ± 19.88	1.77 ± 0.13
CA	Preserved	21	27.56 ± 12.64	9.80 ± 1.17	258.42 ± 20.85	9.02 ± 1.73
	Altered	21	10.41 ± 2.41	3.50 ± 0.68	147.15 ± 19.56	6.23 ± 1.50
	Restored	24	2.21 ± 0.50	1.19 ± 0.10	73.49 ± 9.12	1.49 ± 0.23
VA	Preserved	16	20.77 ± 3.56	84.1 ± 13.21	1513.7 ± 461.7	14.32 ± 9.22
	Altered	24	13.95 ± 3.97	17.67 ± 1.26	286.56 ± 32.97	1.09 ± 0.13
	Restored	21	35.35 ± 9.53	60.16 ± 6.37	703.78 ± 80.30	4.90 ± 0.66
DA	Preserved	24	49.23 ± 10.56	0.52 ± 0.03	137.98 ± 28.56	1.74 ± 0.27
	Altered	12	131.64 ± 45.96	0.66 ± 0.09	290.10 ± 98.31	15.67 ± 4.59
	Restored	24	28.11 ± 6.96	1.40 ± 0.25	237.76 ± 27.71	3.00 ± 0.61
CU	Preserved	24	8.17 ± 1.30	0.53 ± 0.11	124.06 ± 13.90	2.88 ± 0.61
	Altered	24	64.15 ± 7.88	0.32 ± 0.01	217.69 ± 22.22	5.85 ± 0.76
	Restored	24	27.50 ± 4.82	0.32 ± 0.01	137.27 ± 16.38	2.32 ± 0.27

Supplementary references

Christiansen, J. R., Outhwaite, J., & Smukler, S. M. (2015). Comparison of CO2, CH4 and N2O soil-atmosphere exchange measured in static chambers with cavity ring-down spectroscopy and gas chromatography. *Agricultural and Forest Meteorology*, *211–212*, 48–57. https://doi.org/10.1016/J.AGRFORMET.2015.06.004

Hüppi, R., Felber, R., Krauss, M., Six, J., Leifeld, J., & Fuß, R. (2018). Restricting the nonlinearity parameter in soil greenhouse gas flux calculation for more reliable flux estimates. *PLOS ONE*, *13*(7), e0200876. https://doi.org/10.1371/journal.pone.0200876

Hutchinson, G. L., & Mosier, A. R. (1981). Improved Soil Cover Method for Field Measurement of Nitrous Oxide Fluxes. *Soil Science Society of America Journal*, *45*(2), 311–316. https://doi.org/10.2136/sssaj1981.03615995004500020017x

Idzelyte-, R., Cerkasova, N., Mezine-, J., Dabulevičiene-, T., Razinkovas-Baziukas, A., Ertürk, A., & Umgiesser, G. (2023). Coupled hydrological and hydrodynamic modelling application for climate change impact assessment in the Nemunas river watershed-Curonian Lagoon-southeastern Baltic Sea continuum. *Ocean Science*, *19*(4), 1047–1066. https://doi.org/10.5194/OS-19-1047-2023

Rheault, K., Christiansen, J. R., & Larsen, K. S. (2024). goFlux: A user-friendly way to calculate GHG fluxes yourself, regardless of user experience. *Journal of Open Source Software*, *9*(96), 6393. https://doi.org/10.21105/joss.06393

Santinelli, C., Rochera, C., Tropea, C., Schiller, J., Adamescu, M., Ambrosio, R., Attermeyer, K., Bachi, G., Bègue, N., Bučas, M., Cabrera-Brufau, M., Camacho-Santamans, A., Carballeira, R., Carloni, M., Cavalcante, L., Cazacu, C., Checcucci, G., Coelho, P., Dinu, V., … Camacho, A. (n.d.). Hydrological and landscape controls on dissolved organic matter dynamics in European wetlands: Implications for management and restoration. *Submitted to Biogeosciences*.

Silva, J. P., Lasso, A., Lubberding, H. J., Peña, M. R., & Gijzen, H. J. (2015). Biases in greenhouse gases static chambers measurements in stabilization ponds: Comparison of flux estimation using linear and non-linear models. *Atmospheric Environment*, *109*, 130–138. https://doi.org/10.1016/J.ATMOSENV.2015.02.068

Stakėnienė, R., Jokšas, K., Kriaučiūnienė, J., Jakimavičius, D., & Raudonytė-Svirbutavičienė, E. (2023). Nutrient Loadings and Exchange between the Curonian Lagoon and the Baltic Sea: Changes over the Past Two Decades (2001–2020). *Water 2023, Vol. 15, Page 4096*, *15*(23), 4096. https://doi.org/10.3390/W15234096